Measuring 20th century fluvial response to 18-19th century anthropogenic activity using two generations of damming in the South River, western Massachusetts

Author: Samantha Dow

MEASURING 20$^{\text{TH}}$ CENTURY FLUVIAL RESPONSE TO 18-19$^{\text{TH}}$ CENTURY ANTHROPOGENIC ACTIVITY USING TWO GENERATIONS OF DAMMING IN THE SOUTH RIVER, WESTERN MASSACHUSETTS

SAMANTHA DOW

A thesis
Submitted to the Faculty of
the department of Earth and Environmental Sciences
in partial fulfillment
of the requirements for the degree of
Master of Science

Boston College
Morrissey College of Arts and Sciences
Graduate School

May 2018

MEASURING 20TH CENTURY FLUVIAL RESPONSE TO 18-19TH CENTURY ANTHROPOGENIC ACTIVITY USING TWO GENERATIONS OF DAMMING IN THE SOUTH RIVER, WESTERN MASSACHUSETTS

Samantha Dow

Advisor: Noah P. Snyder, Ph.D.

Abstract

Centuries-long intensive land use change in the northeastern U.S. provides the opportunity to study the response timescale of geomorphic processes to anthropogenic perturbations. In this region, deforestation and the construction of dams following European settlement drastically altered the landscape, leading to the impoundment of sediment in mill ponds. This legacy sediment continues to be released into transport decades after a dam has been removed or breached. Geochemical tracers can help distinguish sediment sources and understand how sediment moves through a watershed. The South River in western MA is located in a formerly glaciated watershed, and these surficial deposits compose 98% of the area. It experienced two generations of damming, beginning with smaller mill dams in the 18th-19th centuries, followed by the construction of the Conway Electric Dam (CED), a 17 m tall hydroelectric dam in the early 20th century. Legacy sediment deposits from sediment stored behind mill dams cover 1.5% of the watershed area. The CED is located near the outlet of the river, providing a century-long depositional record for the watershed, during reforestation. I hypothesize that sediment mobilized from human activity will contain a different geochemical signature than glacial material, that recent erosion in the watershed is primarily from anthropogenic legacy deposits rather than from glacial age landforms, and channel widening is occurring in reaches of the channel composed of legacy sediment, rather than in glacially

confined reaches. These hypotheses were tested through a two part investigation, consisting of a sediment tracing study using Hg, and a Geographic Information Systems (GIS) analysis of channel changes using aerial photographs from 1940 and 2014. Samples were collected from river bank exposures of 11 glacial deposits and four mill pond legacy sites. Two vibracores measuring 476 and 500 cm were collected in reservoir sediment stored behind the CED in 2013 and 2017, respectively. Hg concentrations range from 1-4 ppb in glacial sediment, 3-380 ppb in legacy sediment, and 2-18 ppb and 7-50 ppb in the two CED cores. I used Hg as a tracer to estimate percent contributions to the CED reservoir from each watershed source during the 20th century. Results from a sediment mixing model suggest glacial sources contributed $32 \pm 15\%$, and legacy sediment deposits contributed $68 \pm 15\%$ during the 20th century. Based on ^{137}Cs dates on the cores, high amounts of legacy sediment filled in behind the CED prior to 1953 (74 ± 35 %), and background erosion from glacial deposits dominated from 1953 until the reservoir was filled in the 1980s ($63 \pm 14\%$). GIS analyses using aerial photographs from 1940 and 2014 indicate that the channel did not significantly widen along any section of the river, however, increases in sinuosity (up to 12%) occurred in the legacy sediment dominated reaches of the channel, and minor increases (1-2%) occurred in the glacial reaches. Overall, these analyses show an increase in the amount of sediment released in the channel as a result of mill dams breaching through the mid-19th to early 20th centuries, and suggest a short recovery timescale response from this land-use change.

ACKNOWLEDGEMENTS

TABLE OF CONTENTS

LIST OF TABLES

LIST OF FIGURES

1. Introduction

Studies of geomorphic response to perturbations ranging across various spatial and climatic scales such as landslides, floods, or glaciations are common in the literature (e.g., Ballantyne, 2001; Peizhen et al., 2001; Korup et al., 2004; Jackson and Roering, 2009). Recently, humans have been recognized as one of the most important geomorphic agents shaping the landscape (Hooke, 1994), associated with activities such as logging (Ambers, 2001), mining (James, 1999), agriculture (Wilkinson and McElroy, 2007), and the construction of dams (Graf, 1999; Renwick et al., 2005), leading to the movement of sediment from hillslopes to storage in valley bottoms. The extent of anthropogenic disturbance and the timescale over which the landscape will respond to human activity is under inquiry, including how human disturbances compare to background rates of erosion (Reusser et al., 2015).

Dams regulate floods, generate hydroelectric power, provide recreation, and are used for mill operations, yet they also have the potential to alter the landscape by impounding large amounts of sediment mobilized on human timescales, raising local base levels, and decreasing the total sediment flux that reaches the ocean (Milliman and Syvitski, 1992; Syvitski et al., 2005). An increase in sediment loads in rivers over the past several hundred years has been attributed to anthropogenic land use changes, including those mentioned above (Walling, 2006; Wilkinson and McElroy, 2007), and dams have been identified as a solution for the discrepancy between the amount of sediment eroded off the landscape and that reaching the ocean (Syvitski et al., 2005).

Centuries-long intensive land use change in the northeastern U.S. provides the opportunity to study the response timescale of geomorphic processes to anthropogenic

perturbations. Deforestation and the construction of 18th-19th century mill dams on rivers in this region drastically altered the appearance of the landscape and lead to the erosion and impoundment of legacy sediment as a direct result of human activity (James, 2013). Much was deposited in mill ponds and currently persists in valley bottoms, and continues to be released into transport as legacy sediment in rivers throughout the 20-21st centuries, long past when milling operations ceased and after dams breached (Walter and Merritts, 2008; Merritts et al., 2011). Reforestation and recovery from milling operations has been the trend in New England over the past ~150 years. How quickly the channel responds to these disturbances and removes all legacy sediment is unknown. This timescale has important implications for stream restoration and the resilience of this landscape to climate change.

Analyzing sediment geochemistry can identify tracers used to distinguish between sources in order to determine how sediment is moving through the watershed (Walling, 2004; Mukundan et al., 2012). This method will be applied to evaluating 20th century fluvial response to a perturbation from 18th-19th European settlement in New England by studying sediment stored during two generations of damming along the South River in western Massachusetts.

1.1 Prior work on legacy sediment in the Mid-Atlantic region

Major anthropogenic perturbations began during the 1600-1700s in the Mid-Atlantic region of the U.S. with intensive land clearing and cultivation for tobacco and agriculture, leading to high levels of erosion and sedimentation (Costa, 1975). Jacobson and Coleman (1986) distinguish three major stratigraphic units related to land use change

in Maryland, and noted increased sediment supply and runoff related to the most intensive period of agricultural activity from 1730-1930 compared to pre-settlement conditions and post-1930 conditions (trend towards reforestation).

Due to the high density of mill dams in the Mid-Atlantic region, studies on sediment budgets and channel response in valley bottoms were pioneered in 2008 by Walter and Merritts and led to additional work on the subject (Pizzuto and O'Neal, 2009; Schenk and Hupp, 2009; Merritts et al., 2011; Neimitz et al., 2013; Donovan et al., 2016). Legacy sediment accumulated in mill ponds (Walter and Merritts, 2008; James, 2013), and breaching of these dams has led to erosion of the impounded sediment, increasing loads downstream, and leaving 2-5 m high terraces adjacent to the channel (Walter and Merritts, 2008; Pizzuto and O'Neal, 2009; Merritts et al., 2013). Several studies have identified two phases of sediment erosion following dam removal: a 'process driven' phase resulting in a systematic and rapid removal of sediment on the order of weeks to months, followed by an 'event driven' phase, with slow erosion primarily occurring during high flow events (Pizzuto, 2002; Pearson et al., 2011, Collins et al., 2017).

The process of channel widening has been identified as a problem in the Mid-Atlantic region, resulting in sediment pollution and engineering challenges (Galster et al., 2008). Merritts et al. (2013) investigated channel responses occurring several decades after dam breaching; after initial vertical incision, the channel continues to migrate laterally, with sub-aerial processes, mass wasting, and fluvial entrainment acting as the three main erosive processes. Merritts et al. (2013) found that bank erosion occurs during the winter months, primarily due to freeze-thaw processes. Similar lateral migration of the channel through incised legacy sediment has also been noted on annual timescales by

Pizzuto and O'Neal (2009) and with the use of repeat terrestrial LiDAR surveys (Lyons et al., 2015).

Due to high levels of human activity during the 18-19th centuries, high concentrations of trace metals, as well as fertilizers and pesticides were deposited in mill pond sediments in the Mid-Atlantic region (Niemitz et al., 2013). In particular, the South River in Virginia has been noted to store high levels of mercury in channel banks of legacy sediment and floodplains as a result of direct industrial release, and this signal is still seen as high concentrations of Hg in sediment currently being remobilized in the system (Rhoades et al., 2009; Flanders et al., 2010; Pizzuto et al., 2016).

1.2 Legacy sediment in New England

In contrast to the Mid-Atlantic region, few studies have been done in New England, even though both areas experienced similar land use changes during the same era. An important geological difference between the regions is that New England experienced many cycles of glaciation during the Pleistocene, the most recent ending ca. 20,000 years ago, mantling the bedrock with till and other glacial deposits. This leads to different types of sediment available to mobilize in each of the two regions, as the primary source in the Mid-Atlantic is hillslope soil and colluvium developed from the weathering of metarhyolite, sandstone, and quartzite bedrock (Niemitz et al., 2013).

As in the Mid-Atlantic, an increase in agricultural land under cultivation, deforestation, and other land use changes in New England coincided with dam construction (Francis and Foster, 2001), and work using pollen assemblages to reconstruct land use history has indicated higher sedimentation rates after 1700 in

southern Connecticut (Brugam, 1976). Bierman et al. (1997) investigated Holocene rates of hillslope erosion in the sedimentary record of alluvial fans and ponds in Vermont, and noted that the highest rates were linked to European settlement. Thorson et al. (1998) studied sediment stored in Connecticut wetlands as a result of Colonial-era human activity, and the modern landscape is still responding to the large quantity of sediment redistribution experienced during that era.

Little work has been done on the geochemistry of mill pond sediment in New England, particularly concerning Hg and other trace metals. Most studies on Hg distributions related to anthropogenic activities include analyses from cores taken from lakes (Kamman and Engstrom, 2002), off-river bodies (Woodruff et al., 2013), estuaries, and Long Island Sound (Varekamp et al., 2003), where there is a concern for the accumulation of methylmercury in aquatic organisms (Lamborg et al., 2004). Kelleher (2016) compiled a geochemical profile for Hollenbeck Dam in western Connecticut, which was in operation during the second half of the 19th century and contains concentrations up to 40 ng/g of Hg related to anthropogenic activity. However, very little data on concentrations of metals stored in impounded sediment in upland settings exists.

This project explores the response to human perturbation in the South River watershed in western Massachusetts. It is an example of a river in New England's post-glacial landscape that stores a large quantity of legacy sediment as a result of human disturbance during the 18th-19th centuries (Fig. 1; Johnson, 2017). The first generation of dam construction in this watershed began with mills in the 18th century and continued through the 19th century for the purpose of mechanical energy. Many of these structures were subsequently breached from the mid-19th through early 20th centuries. At present,

only two dams remain intact along the mainstem river, and both serve no power generation or water storage purpose. One is the Conway Electric Dam (CED), a larger, concrete dam built in 1906 for hydroelectric power generation. Its downstream location allows it to integrate and record watershed processes. It provides a means to evaluate the processes of 20th century landscape evolution in response to 18th-19th century human perturbations.

1.3 Research motivation and hypothesis

I completed work on sediment transport in the South River for my undergraduate thesis (Dow, 2014). That study focused on quantifying 20th century sedimentation behind the CED and motivated this study in order to evaluate potential sources and contributions of this sediment. Here I address two questions: what is the signature of sediment mobilized by humans, and what was the dominant source of reservoir sedimentation during the 20th century? This thesis tests three hypotheses. (1) Sediment mobilized from human activity contains a different geochemical signature than glacial material, and this signature will allow me to distinguish between these sources. (2) 20th century erosion in the South River watershed is primarily from anthropogenic legacy deposits rather than from glacial-age features. (3) Channel changes and widening along the South River are occurring in legacy-sediment filled valleys rather than in valleys constricted by glacial material.

These hypotheses are tested using two types of analyses. The first component is a sediment tracing study using direct field and lab methods to identify the physical and geochemical properties of sediment from two different sources (glacial and mill pond

deposits) throughout the watershed. The properties of sediment are used as tracers in a mixing model in order to quantify contributions of each source to the CED and will test hypotheses 1 and 2. The second component is a GIS analysis using aerial photographs and LiDAR topographic data in order to map the planform geometry of the river to determine areas of erosion and change since 1940, testing hypothesis 3. These two approaches are used together to identify prominent sources of erosion during the 20th century, and will allow me to evaluate processes of ongoing landscape response to an 18-19th century land use perturbation in a New England watershed.

1.4 Sediment fingerprinting

Sediment fingerprinting, or sediment provenance, is a method that has been used in fluvial environments over the past several decades in order to identify sources at the watershed scale, primarily by analyzing samples of sediment in suspension, but also using samples from river beds, reservoirs, and/or floodplains (Haddadchi et al., 2013). The categories of tracers used to distinguish between different sediment sources include physical characteristics (color, grainsize), bulk geochemistry, mineralogy, mineral magnetic properties, radionuclides, and isotopes (Walling, 2005; Banks et al., 2010). Many studies have utilized mixing/unmixing models as quantitative assessments to statistically evaluate relative contributions of different source areas (Collins, 1998; Banks et al., 2010; Belmont, 2014). Composite fingerprinting, a mixing model using multiple tracers, is a more sophisticated method of combining two or more characteristics of sediment to more accurately distinguish sources and provide better estimates of different source contributions (Mukundan et al., 2012).

Several major assumptions are inherent to sediment provenance studies, and can result in the misrepresentation of the contributions of each of the sources. Tracers used to distinguish sediment are assumed to be conservative in nature (not altered during transport; Belmont, 2014). It is also assumed that the material is moved directly from the source to the sink without the potential for storage during the interim, and that the sink is a representative mixture of all the sources (Collins et al., 2010).

Most provenance studies in New England focus on long timescales, such the deposition of sediment related to previous orogenic events during the Paleozoic (McLennan et al., 2001), or over the Pleistocene and Holocene (Mazzulo et al., 1984). Fingerprinting of fluvial sediment on recent timescales has been focused in areas such as the Mid-Atlantic region (Mukundan et al., 2010) or United Kingdom (Walling 2004; Walling, 2005) with tracers mentioned above. My work attempts to use Hg as a tracer of modern fluvial sediment in New England.

1.5 Geochemical properties of sediment

1.5.1 Hg and other heavy metals

Mercury is a trace metal released both naturally, and as a consequence of human industrial activity, and binds to silts and clays and organic matter before being eroded off the landscape (Varekamp et al., 2003). Current and pre-industrial background levels of Hg in the atmosphere are typically 1-2 ng/m^3, with deposition in soil reflecting these values (Lindqvist and Henning, 1985; Varekamp et al., 2003). Concentrations of Hg found in sediment cores in New Hampshire and Vermont attributed to anthropogenic activity starting ca. 1850 are 2.1 to 6.9 times greater than pre-industrial levels (Kamman

and Engstrom, 2002), and known time periods of Hg release have been used to date sediment deposits (Woodruff et al., 2012; Pizzuto et al., 2016).

Additional metals in the environment that have elevated concentrations as a consequence of human activity include Pb, Cd, Zn, As, Ag, Cu, Cr, and Fe. They are a concern due to their toxicity in low concentrations, and are typically released during mining activities (Duruibe et al., 2007). Coal burning has led to the release of Hg, As, and Cr, among others; oil combustion releases V, Ni, and Sn; the non-ferrous metal industry releases high amounts of As, Cd, Cu, Zn, and Pb (also released from automobile combustion of leaded gasoline); and the iron and steel industry releases Cr and Mn (Nriagu et al., 1988; Pacyna and Pacyna, 2001). These industrial activities lead to increased metal concentrations that primarily enter into the atmosphere and are then cycled through the air, water, and soil.

1.5.2 ^{137}Cs

^{137}Cs is a non-natural fallout radionuclide, signifying sediment deposited after 1953. This date is the start of widespread nuclear weapons testing, and peak concentrations of ^{137}Cs correspond to 1963. At that time, implementation of a ban on nuclear weapons testing caused concentrations to begin to decrease (Mabit et al., 2008). Therefore, ^{137}Cs is useful as a geochronometer and for calculating sedimentation rates during the second half of the 20th century. ^{137}Cs as a tracer has been used to determine erosion from surficial soil under different land uses, and can distinguish between surface (e.g. agricultural land) and subsurface sources (e.g. channel banks), because ^{137}Cs is

concentrated near the surface and decreases with depth (Zapata, 2003; Mukundan et al., 2012).

1.5.3 ^{210}Pb

Excess ^{210}Pb is an atmospheric fallout radionuclide that can be used to determine soil erosion and deposition rates. ^{210}Pb is a natural radiogenic isotope with a half-life of 22.3 years, and is useful in establishing age chronologies and deposition rates over the past ~150 years through the measurement of excess (unsupported) levels. Excess ^{210}Pb is produced from the decay of ^{222}Rn in the atmosphere and is deposited via precipitation or dry fallout, and supported ^{210}Pb is produced in situ in sediment and is in equilibrium with the decay of ^{226}Ra (Zapata 2003; Walling, 2004). ^{210}Pb is typically used as a geochronometer for the past ~150 years, and works particularly well in lacustrine and marine environments, where sedimentation is constant and slow with minimal disturbance (Noller et al., 2000). As a tracer, ^{210}Pb is used in a similar manner as ^{137}Cs, because higher concentrations are located at the surface of the deposit and decrease exponentially with depth.

2. Study area

The South River is located in the towns of Ashfield and Conway in Franklin County, Massachusetts. The river originates in Ashfield Lake, and flows for 25.4 km to its confluence with the Deerfield River. This upland watershed encompasses 68 km^2, and the average gradient is 0.004 m/m (Field, 2013). The bedrock geology is characterized by the Conway Formation, a group of Devonian age mica-schists interbedded with limestone

(Emerson, 1898). Glacial deposits along the South River include till and coarse stratified deposits (Stone and DiGiacomo-Cohen, 2010; Fig. 2). Field work has indicated that the stratigraphy of many of the glacial exposures along the river are composed of lodgement till up to several meters thick, overlain by a 2-3 m layer of glacio-fluvial sand (Fig. 3). An excavated sand pit in the town of Ashfield indicates the presence of a glacial-age delta (Fig. 3), and provides evidence of a small glacial lake filling the upper South River valley after the last glaciation (a second one may have filled the lower valley), as speculated by Emerson (1898) and Stone and DiGiacomo-Cohen (2010).

Conway and Ashfield are historically agricultural towns, and farming is the primary economic activity. These towns were largely deforested during the 18th-19th centuries, with a majority of land use devoted to pasture. In 1830, Conway was ~20% forested, whereas Ashfield was ~7% forested (Foster and Motzkin, 2009; Fig. 4). Both towns experienced ~50% reforestation near the beginning of the 20th century, increasing to ~80% reforestation during the mid-20th century, remaining consistent through the present (Office of Geographic Information, MassGIS; Fig.4; Tables 1 and 2).

The first mill was constructed on the South River in Ashfield in 1744, and as many as 30 throughout the watershed were operational until the 20th century; they included grist, saw, cider, and fulling mills (Pease, 1917; Howes, 1910; Field, 2013). The height of manufacturing along the river occurred from ca. 1830-1870 in the center of Conway. The primary industry was textiles, however various smaller operations such as precision metals and cutlery existed (Pease, 1917). Manufacturing was phased out along the South River during the early 20th century and the majority of dams were abandoned by 1921 (Barten and Kantor, 2013), with no notable industrial activity occurring along

11

the river over the past 100 years. Today, Conway and Ashfield remain primarily agricultural and residential towns.

Sediment accumulation in mill ponds accounts for a volume of up to $2.5 \times 10^6 \, m^3$ of material stored in legacy sediment terraces, covering 1.5% of the watershed area (Johnson, 2017). Typical stratigraphic profiles of legacy sediment in the watershed include massive sand and silt layers that range from 40-219 cm thick, some of which are underlain by gravel and cobbles, interpreted as the pre-dam river bed (Johnson, 2017). No layers of Holocene organic wetland soil that are commonly found in the Mid-Atlantic region have been discovered underlying the legacy sediment (Walter and Merritts, 2008; Johnson, 2017).

Mill dam sedimentation along the river reflects human activity during the 18-19th centuries. Mercury is expected to have been introduced in high concentrations in the watershed because of manufacturing activities. A potential source of Hg is a hatting shop that was located in the center of Conway (Pease, 1917; years of operation unknown, likely early 1800s). Hg would have bound to sediment that was transported in the river and deposited behind mill dams. Bank exposures along former mill ponds are likely sources of sediment erosion during the 20th century, releasing potentially contaminated sediment back into the watershed.

Additional human modifications to the channel include straightening and widening starting during the mid-1800s in response to flooding and the potential for dam breaching; up to 17,100 m or 67% of the channel was straightened prior to 1886 (Field, 2013). The Great Freshet flood of 1869 resulted in the damage of several dams in the center of Conway; these structures were rebuilt by 1871 (Barten and Kantor, 2013). The

dam at the outlet of Ashfield Lake breached in 1878 resulting in vast damage downstream along the channel. The region was impacted by large hurricanes in 1904, 1936, 1938, 1955, and 2011 each causing severe flooding (Fig. 5). The Tucker and Cook Dam located just upstream of Conway's town center was dismantled in 1936 following flooding from the hurricane (Fig. 6; Barten and Kantor, 2013). These large events during the late 19th-early 20th centuries likely resulted in the breaching of other dams along the channel. Armoring and bank stabilization took place during the 20th century in response to several large flood events, including flooding during Tropical Storm Irene in 2011 (Field, 2013). Field (2013) estimated that approximately 25% of the banks are currently undergoing erosion, with glacial sources and mill pond deposits being primary contributors to high sediment loads.

The Conway Electric Dam is a 17 m tall dam located on the South River downstream of these glacial and mill pond deposits, and 1 km upstream from the confluence with the Deerfield River (Figs. 1 and 3). It was originally constructed in 1899 as a wooden dam, and replaced by a concrete structure in 1906 to generate hydroelectricity to power a trolley (Pease, 1917; Field, 2013). Being located near the outlet, the CED acts as a trap for sediment from the entire watershed. Aerial photographs suggest the dam was completely filled in by 1981 (Fig. 7; Dow, 2014). Sediment yield estimates calculated in the South River indicate two possible trends in sedimentation during the lifetime of the dam from 1906-1981, where sedimentation decreases overtime, or potentially displays a large peak in sediment moving through the watershed from 1940-1952 (Fig. 8; Dow, 2014).

Four vibracores (VC1, VC2, VC3, and VC4) were collected on the left bank floodplain ~50 m upstream of the CED in 2013 (Fig. 7; Dow, 2014). All cores were sampled in ~10 cm intervals for geochemical, loss on ignition (LOI) and grainsize analyses. Geochemical analyses included measurements of concentrations of Hg, ^{137}Cs, and ^{210}Pb, and were focused on Vibracore 3 (VC3; 473 cm long) as it had the deepest recovery. Hg, ^{210}Pb, and ^{137}Cs are present within the top five meters of sediment at the site (the deposit may be up to 17 m thick, but our coring method could not obtain a sample this long; Figs. 9 and 10). An age model determined from ^{137}Cs suggests that this sediment is younger than 1953. Fine-grained (silt/clay) sediment was sampled between 200-473 cm depth for Hg; measured concentrations ranged from 2-18 ppb. Hg detected in sediment behind the Conway Electric Dam is likely to be related to 19th century manufacturing in the watershed, derived from remobilized legacy sediment from eroding mill pond deposits.

3. Methodology

3.1 Sediment sample collection

Sites for sampling legacy and glacial sediment were selected based on interpretations of features in LiDAR imagery and mapped legacy sediment terraces by Johnson (2017; Fig. 1). GPS locations of the sites were obtained using a handheld Trimble Juno SB unit and a Leica Viva GNSS GS14 Rover. Sediment samples were collected during the summer of 2016 from banks of various actively eroding glacial and mill pond sources along the mainstem South River (Fig. 3). These are areas where visible erosion is occurring along the channel, and evidence of mass wasting has been noted

14

during and after high flow events. It is assumed that the major source of sediment entering the channel is directly from the banks and adjacent deposits. The surface of in situ glacial deposits was scraped off and fresh samples were collected. Four bank exposures of mill pond deposits were cleaned off to reveal a fresh face and were sampled in 10 or 20 cm depth intervals. Samples for bulk density analysis were collected from mill pond deposits in half meter increments using a syringe. Fine-grained sediment in the river channel was collected for analysis of sediment currently in active transport. Munsell soil color descriptions and codes were assigned for moist samples of mill pond and glacial sediment.

An additional vibracore (VC5) measuring 500 cm was collected in the Conway Electric Dam reservoir sediment in May 2017. It is located upstream in the deposit of the cores taken by Dow (2014) (Figs. 7 and 10).

3.2 Grainsize and geochemical analyses

Preparation of samples for grainsize and geochemical analyses was conducted at Boston College. Samples were dried at 60°C and split for geochemical and grainsize analyses using the coning and quartering method. Loss on ignition (LOI) analysis to determine organic carbon content was then conducted on dried samples using standard procedures (Dean, 1974). Post-LOI samples were dispersed using 0.2% sodium metaphosphate, then wet-sieved at 63 μm to obtain the weight percent for the <63 μm fraction. Sediment in the >63 μm fraction was analyzed for grainsize at the University of Connecticut using a Horiba CAMSIZER-L Digital Image Processing Particle Size Analyzer in order to obtain weight percentages in 100 size classes from 63 μm-1 cm.

Cumulative grainsize distributions and D_{10}, D_{50}, and D_{90} values (the grainsize for the percentage of the sample finer than this value) for the entire distribution (<63 μm fraction added to the >63 μm fraction) were calculated using the program Gradistat Version 8.0 (Blott and Pye, 2001).

Dried samples were homogenized for Hg, ^{210}Pb, ^{137}Cs, and XRF analyses by powdering with a mortar and pestle. Direct combustion analyses for Hg were conducted at Amherst College using a Teledyne Leeman Labs Hydra-C mercury analyzer with cold vapor atomic absorption (CVAAS). Generally, samples with D_{50} >200 μm were not analyzed for Hg, as Hg does not concentrate on coarser sediment due to low surface area. Therefore, measurements were focused on finer sediment because it has a higher surface area for metals to adsorb to (Horowitz and Elrick, 1987). Hg concentrations were normalized to organic content obtained from LOI. ^{210}Pb and ^{137}Cs concentrations were analyzed using gamma spectrometry at UMass Amherst on a Canberra GL2020R Low Energy Germanium Detector gamma counter. X-ray fluorescence (XRF) analyses for 33 elements (Mo, Zr, Sr, U, Rb, Th, Pb, Se, As, Hg, Au, Zn, W, Cu, Ni, Co, Fe, Mn, Cr, V, Ti, Sc, Ca, K, S, Ba, Cs, Tb, Sb, Sn, Cd, Ag, and Pd) were completed at the University of Connecticut. Approximately 1-2 g of homogenized sediment was placed into capsules and elemental concentrations were measured using a Thermo Scientific Niton XL3 Analyzer handheld XRF gun.

3.3 Sediment mixing models

3.3.1 Tracer determination

Tracers that display non-conservative behavior or are unable to distinguish between sources are eliminated through statistical determination. These criteria were used in this study to determine the utility of potential tracers. The measured property used as a tracer in the sink must fall within the ranges of the sources. The usefulness of tracers in distinguishing individual sources is determined statistically through the use of methods such as the Kruskal-Wallis H-test, Wilcoxon Rank Sum test, or Mann-Whitney U test. The Mann Whitney U test was used in this evaluation, with significance at the 95% confidence interval. In order to be useful as a tracer, that characteristic property must be significantly distinguishable for each of the sources. An additional step includes a stepwise discriminant function or a principle component analysis when dealing with multiple tracers to determine a fingerprint including the optimal combination of parameters (Miller et al. 2015). Due to the limited number of tracers and sources used in this model, this step was not performed.

^{137}Cs, ^{210}Pb, grainsize, and Hg were evaluated for their usefulness as tracers based on the criteria above. Only Hg was found to statistically distinguish between the different source types, and thus was the only tracer included in the mixing model. ^{137}Cs was not detected below ~20 cm in the mill pond deposits, and none is assumed to be found in glacial sediment; it was therefore not used as a tracer because it is not consistently found throughout the mill pond deposit, and is unable to distinctly distinguish this source from glacial sediment. ^{210}Pb was detected in legacy and CED sediment; however, uncertainty in measurements is large. Since no glacial samples were analyzed for ^{137}Cs or ^{210}Pb as neither are expected to be present, this tracer was not used due to the lack of data.

3.3.2 Two-end member model using Hg

A two-end member mixing model was used to calculate relative contributions of legacy and glacial sources to the Conway Electric Dam deposit using their average Hg concentrations as a tracer. The percent contributions for each source are expressed by:

$$\sum_{j=1}^{m} x_j = 1; \ \ 0 \le x_j \le 1. \hspace{2cm} (1)$$

The unknown contributions are solved by:

$$\sum_{j=1}^{m} a_{i,j} x_j = b_i, \hspace{2cm} (2)$$

where x_j is the unknown weighted percentage of source j contributing to the representative deposit, or the sink, $a_{i,j}$ is the average concentration of the tracer i for each source j, b_i is the average concentration of tracer i in the representative deposit, m is the number of individual sources (Small, 2002; Palazón et al., 2015).

The mixing model was solved using Hg as the tracer, i ($i=1$). The number of sources is $m=2$, where the two sources, j, are the legacy and glacial deposits. It is assumed that average concentrations of each tracer can be used since this represents an average mixing of all of the sources equally to the sink (Collins et al., 2010). Hg is assumed to display conservative behavior, and not change forms while in transport. Sediment is also assumed to be eroding directly from adjacent channel banks, where visible active erosion is occurring, and deposited to the CED directly, without any storage in bars or floodplains along the channel, which is reasonable because the analyses focus on sediment <200 μm, which largely travels as suspended load in the gravel-bedded river.

18

3.3.3 Handling uncertainty

Uncertainty in the mixing model arises from various causes, including the sampling process, natural heterogeneities among similar sources, selection of tracers, and instrumental measurements (Small et al., 2002). The sampling process can result in uncertainty due to limits on the number of samples collected and resources for analyses. Propagation of error in mixing models is typically accomplished with Monte Carlo methods.

The measured concentrations of Hg for each of the sources and sink at the South River vary over two orders of magnitude, and appear to be log-normally distributed (Fig. 13). Uncertainty was propagated through Monte Carlo methods, using the average and standard deviation Hg concentrations of the log normal distributions to generate 10,000 random possible end-member concentrations. The log transformed Hg values were taken out of log space and returned to normal concentrations in ppb before being incorporated into the mixing model.

3.4 GIS aerial photograph analyses

Changes in the channel width were evaluated using aerial photographs from June 1940, orthoimagery from April 2014 (30 cm resolution), and LiDAR DEMs from 2012 (2 m spatial resolution) and 2015 (1 m). The 1940 aerial photographs (original scale 1:24,000) were georeferenced in ArcGIS using a spline transformation with a minimum of 10 ground control points (GCPs), resulting in minimal residual error (less than 1%). Spatially referenced road intersections were used as primary GCPs. Right and left channel banks were manually delineated from the aerial photographs.

Channel bank types were mapped along the river and divided into glacial (including minor sections of bedrock channel located in the downstream reaches) and legacy sediment reaches (Fig. 3). Mapping was done using interpretations from a combination of LiDAR features, GIS-based identification of legacy sediment terraces (Stout and Belmont, 2014; Johnson, 2017), and field observations in order to calculate the length of each type of bank exposure.

The channel was divided into six reaches based on changes in valley width (Fig. 11). The widths across the valley were measured in 100 m increments along the length of the channel. The average width across the valley is 204 m. Sections where the valley is <200 m were classified as narrow, constricted reaches, where sections >200 m were classified as wide reaches. This grouping corresponds with segments of the channel mapped by Johnson (2017) that are composed of legacy or glacial sediment, where the narrow reaches are confined by glacial deposits, and the wide reaches have been filled in with legacy sediment. The channel upstream of Reach 6 to its source at Ashfield Lake becomes narrow and highly vegetated in the aerial photographs, and was unable to be digitized and used in the evaluation.

Channel width was then measured for each set of aerial photographs. The mainstem of the river was divided into 80 m lengths to maximize the number of measurements while ensuring that measurement intervals were far enough apart to remain independent of each other (Galster et al., 2008). Widths across the channel were measured for both sets of aerial photographs. Areas with heavy vegetation or where the channel became too narrow to delineate were excluded from the analysis.

20

Changes in channel width were calculated by subtracting the 1940 width from the 2014 width. Two sample t-tests were used to determine if significant changes exist in the difference in width for each reach type between the two time intervals for the entire channel as a whole. T-tests were then used to determine if significant width changes occurred in each individual reach between the two time intervals.

Changes in sinuosity were determined for each individual reach, by dividing the length of the measured channel by the straight distance along the reach (Edwards and Smith, 2002). The length of the right and left bank of each reach were averaged to obtain the channel length. The straight distance was measured as the shortest path between the start and end of the channel in each reach segment.

For a more recent comparison, the 2012 and 2015 LiDAR datasets were differenced in ArcMap to generate a map showing areas of erosion and deposition for the entire watershed. The 1 m 2015 LiDAR was converted into a 2 m DEM to match the cell resolution of the 2012 data set using the ArcGIS tool Extract by Mask. The two years were differenced by using the Minus tool to generate a new raster containing data on the elevation change.

4. Results

4.1 Grainsize analyses

The material composing legacy sediment deposits primarily consists of silt and sand, with an average D_{50} of 115 µm (69-189 µm, 1σ range) (Fig. 12; for average grainsize of each deposit see Table 3). The average D_{50} of all the glacial sediment collected is 104 µm (62-174 µm, 1σ range). Mann-Whitney U tests indicate no statistical

difference in grainsize between legacy and glacial deposits (p=0.4145). The average D_{50}

of sediment analyzed for Hg in VC3 is 54μm (28-105 μm, 1σ range), and 97μm (59-158

μm, 1σ range) for VC5, and the average for the combined samples in the two cores

analyzed for Hg is 77 μm (41-144 μm, 1σ range). The range of the minimum D_{50} of the

CED (18 -159 μm) does not fall within the observed range of either the legacy (28-291

μm) or glacial deposits (46 – 209 μm). Therefore, it is unable to be used as a tracer.

4.2 Hg analyses

Measured Hg concentrations in glacial samples (1-4 ppb; average 2.06 ppb) are

lower than in legacy sediment (3-380 ppb; average 13.36 ppb; Fig. 13; Table 4). Mann-

Whitney U tests indicate a statistical significance between the means of the two deposit

types (p = 1.49 x 10^{-6}). The concentrations for glacial deposits can establish a pre-

anthropogenic baseline of Hg levels. Profiles from three of the four legacy sites (MPSR1,

MPSR4, MPSR5) have concentrations ~10-20 ppb (Figs. 14-16). The farthest

downstream site (MPSR2) has higher concentrations, with a peak of up to 380 ppb

occurring at ~100 cm depth (Fig. 17). Influences on Hg concentrations by grainsize or

organic content were evaluated, however, both demonstrate no or weak correlation (Figs.

18-20). Concentrations from core VC3 at the Conway Electric Dam reservoir indicate

values from 2-18 ppb (average 6.30 ppb) from depths 200-500 cm below the lake bed

(Fig 9). Concentrations measured in VC5 are 7-50 ppb (average 15.99 ppb) from the

surface to 500 cm below the lake bed, and are statistically lower in the core (two sample

t-test, p = 0.0014; Fig. 21). Relationships between Hg, grainsize, and LOI were explored

for VC3 and VC5, and are also not or weakly correlated (Figs. 22 and 23). Most active

channel samples collected were too coarse to run for Hg (D_{50} >200 μm), however two samples that were analyzed had concentrations of 8-9 ppb (more consistent with the range of those at the Conway Electric Dam; Table 5).

4.3 ^{210}Pb and ^{137}Cs analyses

^{137}Cs and ^{210}Pb were measured at the four legacy sites. Three samples were evaluated at each bank exposure, one near the top at 15-20 cm depth, one at ~ 100 cm depth, and one near the bottom at ~180 cm depth (Figs. 14-17; Table 6). ^{137}Cs is present within the top 20 cm of the legacy deposits in concentrations from 3-12 Bq/kg, with no ^{137}Cs detected in measurements made below 100 cm depth. In addition, site MPSR2 was sampled from 10-40 cm depth to obtain a more complete record near the surface. ^{137}Cs was detected in all of these samples in concentrations of 0.6-15 Bq/kg (Fig. 17; Table 6). A peak in ^{137}Cs occurs at 30 cm depth in this profile, and assuming that the peak corresponds to the age of 1963 and no downward diffusion of ^{137}Cs, it results in an overbank sedimentation rate of 56 cm/100 years in the former millpond.

Excess ^{210}Pb was detected in the sediment at all depths, ranging from 37-90 Bq/kg. However, due to the short time span over which the mill ponds filled in with sediment, ^{210}Pb in this system displays variability rather than an exponential decay, making it unreliable for use as a geochronometer or for calculating sedimentation rates. The limited analyses also result in an incomplete profile of ^{210}Pb for these sites.

^{137}Cs was analyzed on VC5 at 154, 421, and 487 cm depth. No ^{137}Cs was detected in any of these samples, providing an age older than 1953 for sediment below 154 cm depth.

4.4 XRF analysis

XRF analyses were conducted for the MPSR2 profile and four glacial samples. Concentrations of 11 elements were detected in all samples (Zn, Zr, Sr, V, Fe, Ca, K, Ti, Rb, Sc, Mn) and show little variability throughout the profile of MPSR2, as well as between glacial and legacy deposits (Fig. 24; Table 7). Sixteen elements were not detected in any of the legacy or glacial samples (U, Se, As, Hg, Au, W, Ni, Co, Ba, Cs, Te, Sb, Sn, Cd, Ag, Pd), and six were detected in some legacy or glacial samples, but not all (Mo, Th, Pb, Cu, Cr, S; Table 8). Elements associated with anthropogenic activity (Pb, As, Cr, Cu) were either below the level of detection, not consistently found in all legacy samples, or were detected in low concentrations that did not exceed those measured in the glacial sediment. These elements were not detected in the glacial material either.

XRF for VC5 detected 12 elements in all samples throughout the entire depth of the core (Zr, Sr, Rb, Th, Zn, Fe, Mn, V, Ti, Sc, Ca, K), 11 elements in some samples, but not all (Mo, U, Pb, As, Cu, Ni, Cr, S, Ba, Cs, Sb, Hg, Co, Te, Sn), and six elements were not detected in any of the samples (Se, Au, W, Cd, Ag, and Pd) (Table 9). Elements that may be associated with anthropogenic activity detected in VC5 but not mill pond or glacial samples include Pb (0-36 ppm), As (0-6 ppm), and Ni (26-51 ppm).

4.5 Mixing model calculations

The mixing model analysis was completed using Hg concentrations from both VC3 and VC5 to represent the CED and to calculate the overall contribution over the lifespan of the dam. From this analysis, 32 ± 10% of the CED deposit is from glacial sources and 68 ± 10% is from legacy sources (Table 10). A sensitivity analysis on the

data was used to evaluate contributions for the entire deposit by excluding the two highest outliers in the mill pond data (367 and 380 ppb; Fig. 17). Results from this analysis indicate that glacial sources contributed $15 \pm 36\%$ and legacy deposits contributed $85 \pm 36\%$ (Table 10).

Because the presence or absence of ^{137}Cs signifies deposition before or after 1953, it allowed for the breakdown of the mixing model to analyze source contributions from the first and second halves of the 20th century. Hg concentrations from 154-500 cm in VC5 are from sediment deposited prior to 1953; it is assumed concentrations from the top 154 cm were deposited after 1953, and known that the entirety of VC3 is younger than this age (Figs. 9 and 21). The separation of these two periods suggest that $26 \pm 35\%$ is from glacial and $74 \pm 35\%$ is from legacy deposits prior to 1953. After 1953, $63 \pm 14\%$ is from glacial and $37 \pm 14\%$ is from legacy deposits (Table 10). A sensitivity calculation performed in the same manner as outlined above was used in evaluating pre and post-1953 contributions. This calculation suggests that before 1953, $8 \pm 40\%$ is being contributed by glacial material, and $92 \pm 40\%$ is from mill ponds. After 1953, this transitions to $54 \pm 15\%$ from glacial material and $46 \pm 15\%$ from mill ponds.

4.6 Channel width and sinuosity analysis

Statistical analysis using two sample t-tests on changes in width indicate no significant changes in width overall for reaches with legacy sediment banks (p= 0.4262), and the average change as 0 ± 4 m (Fig. 25, Table 11). Changes in the glacial sediment reaches are significant (p < 0.05) and overall display a narrowing trend of -3 ± 6 m. Each

individual reach was also analyzed for changes. Reaches 5 (legacy) and 6 (glacial) both display narrowing of -4 ± 6 m and -3 ± 2 m, respectively. The period of the photographs excludes the first 40 years of the 20th century, so any dam breaches or erosion during this time cannot be accounted for in this analysis.

Change in sinuosity was calculated for each of the reaches. Overall, the narrow reaches composed of glacial material have experienced a minimal increase in sinuosity (1-2% change). The legacy sediment sections indicate increased sinuosity of up to 12%, except for Reach 2, where no change in sinuosity has occurred (Table 11).

5. Discussion

5.1 Characterization of sediment sources

Glacial sources in the watershed provide a pre-industrial geochemical baseline for trace metals to compare with the signal of sediment mobilized on anthropogenic timescales. Buried glacial material not in contact with the atmosphere has not been exposed to the fallout of high concentrations of trace metals (such as Hg) associated with industrialization. It therefore provides background levels of trace metals in sediment for the watershed, containing lower concentrations of Hg (1-4 ppb) than sediment mobilized since industrialization (3-380 ppb; Fig. 13). As most of the surficial sediment in the watershed is till (Fig. 2), essentially all of the sediment in transport in the South River is originally glacial, whether directly mobilized or reworked. However, despite the glacial origin, different geochemical signatures reflect sediment mobilized and deposited during different times.

Higher concentrations of Hg in legacy sediment than glacial sediment is likely attributed to an increase in global atmospheric concentrations produced from coal burning and other industrial activity beginning ca. 1850 (Perry et al., 2005; Kamman and Engstrom, 2002). These elevated levels represent higher atmospheric concentrations and airborne pollution from factories falling out over the landscape, and generally range from ~10-20 ppb in the legacy deposits (Fig. 13). The high concentrations of up to 380 ppb of Hg at MPSR2 are likely related to local point source pollution (Fig. 17). A hatting shop located in the center of Conway upstream of this site (Fig. 1) during the early 19th century is a likely explanation, as mercury nitrate was used in the processing of fur in the hatting industry (Pease, 1917; Varekamp, 2006). Higher concentrations at this site could also be a result of its downstream location, as it accumulates the signal of many upstream sources with lower Hg concentrations.

MPSR4 is also located downstream of the hatting shop in the same reach of river as MPSR2, however, it does not display a similar Hg profile with high concentrations of Hg (Figs. 15 and 17). Discrepancies in these sites could arise as a result of the timing of infilling behind the dams and the timing of the release of Hg from its point source. The millpond at MPSR2 may have been filling in during favorable conditions to capture the signal, where MPSR4 may have been filled in prior to or after the period of contamination release. An additional discrepancy between sites could be a function of grainsize; However, while MPSR4 is slightly finer grained than MPSR2 (Table 3), there is no statistical difference between the grainsize at the two sites (Mann-Whitney U test, $p=0.7032$), and cannot account for the significantly higher amounts of Hg detected in MPSR2.

Results from XRF indicate that additional trace metals related to anthropogenic activity (Pb, Cu, As) were not detected in legacy sediment (Table 8). No direct releases of these metals or their usage have been documented for the watershed during the 18th-19th centuries. Concentrations of these metals were not detected in glacial sediment either. However, it cannot be ruled out that concentrations of these elements exist in the sediment but are too low to be detected using this method, or are influenced by grainsize effects of the sediment.

The deposit behind the CED gives a chance to characterize sediment that accumulated during the 20th century. This sediment is derived from a mixture of both glacial and mill pond deposits, and the sediment from these sources has the potential to become contaminated with trace metals during remobilization. XRF results from VC5 show elevated concentrations of Pb and Ni, which may be related to 20th century anthropogenic activity, as these elements were not detected in mill pond or glacial samples (Table 8). Elevated Pb levels during the 20th century began ca. 1920 with the use of leaded gasoline (Neimitz et al., 2013), and the detection of Pb in this core is consistent with the reservoir sediment being deposited during 20th century.

Cr is detected in lower concentrations in the mill pond sediment (15-46 ppm) than glacial (50-66 ppm; Table 8), and falls within the ranges of these two sources in the CED (12-75 ppm; Table 9). It has the potential to also be used as a tracer in this system, however, additional concentrations in glacial samples, other legacy sites, and VC3 would need to be analyzed to get a more complete dataset for this source before being utilized as a tracer.

5.2 GIS channel analysis

The channel change analysis is limited by several factors including aerial photograph quality (color and scale), vegetation, and georeferencing. The 1940 images are in black and white and have a lower resolution (2 m) than the 2014 data set (30 cm). This makes delineating the channel difficult in some sections of the watershed, resulting in greater interpretation in mapping and less accuracy.

Channel narrowing exhibited by the glacial reaches should be viewed with caution, particularly upstream (e.g. reaches 5 and 6; Fig. 11) where the channel is relatively narrow and obscured by vegetation. The quality of the 1940 aerial photographs and georeferencing process may inaccurately represent channel changes, and result in greater error in width measurements. Narrowing may also be caused by the time of year the photographs were taken, due to tree cover or differences in seasonal or yearly discharge conditions (i.e. a drought during one of the years). Monthly average discharge recorded at USGS stream gage 01168500 along the Deerfield River for June 1940 was 26.4 m^3/s. For April 2014, the monthly average was 54.7 m^3/s (USGS, 2017). This gauging station was chosen for use due to its proximity to the South River and its record beginning in 1913; stream gage 01169900 along the South River begins its record in 1966, which does not encompass the 1940 imagery (Fig. 5). The lower discharge in 1940 could cause the water level to appear lower and have a narrower width in the image, however, this scenario should result in the appearance of widening. Therefore, it is unlikely that discharge differences between these two years can account for the narrowing.

Sinuosity measurements indicate that the legacy sediment sections of the channel, while not exhibiting significant changes in width, are still dynamic and migrating (Table 11). The increase in sinuosity suggests it is currently acting as a meandering river in the sections of legacy sediment, as these legacy terraces occur in wide sections of the valley, and the river therefore has room to migrate.

Results from the LiDAR differencing are also to be viewed with caution. The differenced raster contains background noise that appears to be aspect dependent. It suggests an overestimate in the amount of deposition, which could be caused by offset or other processing issues in the datasets (Fig. 26). Overall, few places where more than a meter of erosion or deposition have taken place in the watershed, however, no major floods that may have caused significant erosion occurred between 2012 and 2015; no notable flooding events have occurred since Hurricane Irene in 2011 (Fig. 5).

5.3 Changing sediment sources in the CED deposit

Overall, the mixing model using data from cores VC3 and VC5 suggest contributions to the CED deposit of legacy sediment sources are higher than glacial (Table 10). These variations in concentrations of Hg at different sites, in particular the prescence of a few high concentrations at MPSR2, lead to uncertainty in the mixing models (Fig. 1; Fig. 17). The sensitivity analysis removed the two highest Hg concentrations in the legacy sediment (367 and 380 ppb), as these concentrations may bias contributions toward less pond sediment, but results suggest even higher mill pond contributions of 85 ± 36%. Increasing the sampling distribution and including more legacy sites could change the outcome of the mixing model depending on factors such as

30

proximity of the location to the source of Hg release, which would influence

concentrations at that site. In contrast, concentrations in the glacial sediment are low (Fig.

13), so increasing the number of samples taken probably would not drastically alter the

range of concentrations of Hg measured in this source.

The concentrations of Hg in the CED deposit increase with depth and age in the

cores, which could represent a change in the dominant source of sediment over the

lifespan of the dam (Figs. 9 and 21). The VC5 Hg profile shows statistically lower

concentrations (two sample t-test, p= 0.0014) in the top 100 cm of the core (7-12 ppb)

than the bottom (11-50 ppb). Higher concentrations in older sediment (pre-1953 based on

the lack of ^{137}Cs) from the bottom 154 cm of VC5 (11-50 ppb) suggest more erosion from

mill pond deposits earlier in the CED's history. The Hg concentrations in the top half of

VC5 are comparable to the concentrations found throughout VC3 (2-18 ppb), and suggest

a slowing of erosion from mill pond deposits after 1953. I assume that the top 154 cm of

VC5 was deposited after 1953, as Hg concentrations in this part of the core are similar to

those in VC3, although testing this would require running ^{137}Cs analyses from samples in

this interval.

High legacy sediment contributions earlier in the CED's history is suggested in

the mixing model from sediment pre-1953, with a transition to glacial material after 1953

(Table 10). Sensitivity analyses on these periods also suggest that contributions of mill

pond sediment into the CED is extremely high (up to 92%) before 1953, with a transition

to more glacial material filling in behind the dam after 1953. Results from the post 1953

sensitivity analysis are not as drastic though, and suggest that erosion from the two

sources could be relatively equal, about 50% each. Overall, the sensitivity analysis

demonstrates the same trend as the original mixing model, but it can provide some probabilistic constraints on percent contributions from each of the sources.

Many of the mill dams in the watershed were abandoned by 1921, and likely breached during the mid-19th through early 20th century, particularly related to some of the large floods (1869, 1904, 1936, and 1938; Barten and Kantor, 2013; Fig 5). One example, the Tucker and Cook Dam (MPSR5 samples collected at this location; Fig. 1), built in 1837, was removed in 1936 following a large storm event (Barten and Kantor, 2013; Fig 6). This is likely one among one of the last historic dams that was removed or breached, as there is little evidence of remaining dams and reservoirs in the 1940 aerial photographs. This may have resulted in a pulse of legacy sediment moving through the watershed, with high levels of Hg, before erosion from these deposits slowed through time. It is likely that the CED records this pulse of sediment from dams that breached during the first few decades of the 20th century, with the relative contribution of legacy sediment decreasing through time as erosion from these deposits slowed. However, this time period is not captured in aerial images, and the GIS analysis does not encompass significant changes in channel width that would have occurred upstream of the dams right after breaching. This lack of documentation occurs during a time when the channel may have been more dynamic and more erosion from banks of legacy sediment would have been occurring, leading to higher sedimentation behind the CED.

The erosion of sediment following dam removals has been described through "process driven" and "event driven" erosion (Pizzuto, 2002), and these stages have been observed at low head dam removal sites throughout the U.S. (Sawaske and Freyberg, 2012; Major et al., 2017). Dam removal monitoring done at the Merrimack Village Dam,

New Hampshire, and Simkins Dam, Maryland, show two stages of sediment removal, where the first stage ('process driven' phase) occurs quickly within weeks to months after the dam has been removed, followed by the 'event driven' phase where erosion slows and sediment is primarily removed from the former impoundment during high flow events (Pearson et al., 2011; Collins et al., 2017). Collins et al. (2017) suggest that the removal of sediment from the impoundment can be described by two different exponential equations representing each of the above phases. Erosion of sediment from behind mill dams in the South River likely follows a similar trend, and current erosion is now in the 'event driven' phase where sediment erosion off of exposed banks occurs primarily during high flow events.

I have the opportunity to study the response over decades, compared to the monthly or yearly timescale of most dam removal studies. Pizzuto and O'Neal (2009) find evidence for accelerated bank erosion rates along the South River in Virginia in the decades after mill dam breaching, and similar trends have been observed and modelled for breached mill dams along Hammer, Mountain, and Conoy Creeks in the Mid-Atlantic region, where sediment production from banks over a decadal timescale follows a negative power function, where the highest amount of sediment is released within the first decade following dam removal (Merritts et al., 2013). However, most studies focus on a much shorter timescale of removal. This study links sediment removal from behind two generations of damming on a decadal to centennial timescale.

Previous studies observe that on a monthly to yearly timescale of dam removal, about 50% of the total volume is removed from non-cohesive (sand and gravel) deposits in less than two years, and it takes greater than two years for cohesive (mud, clay)

33

deposits (Sawaske and Freyberg, 2012; Major et al., 2017). Trends in sediment removal from behind breached mill dams in the South River likely follow a similar pattern based on findings from these studies, and erosion of 50% of the total volume is expected to take about two years, as mill pond sediment is primarily silt and fine sand.

While many glacial sources are located far upstream, there are several 30-40 m thick exposures located within 3.5 km of the CED (Fig. 1), which may contribute large amounts of sediment. These exposures have displayed evidence of mass wasting during large storm events such as Tropical Storm Irene in 2011 (Field, 2013), exhibiting this "event driven" bank erosion, and are still an active source of sediment throughout the 20-21st centuries. Dethier et al. (2016) found that banks composed of glacial material along other rivers in Vermont and western Massachusetts continue to release sediment from landslide scarps adjacent to river channels years after Irene, and fine grained sediment from these exposures remains available for transport even under low flow conditions. Mixing model results in this study suggest that there is a transition to glacial sources being the primary contributor of sediment in the latter half of the 20th century (Table 10). Overall, only 1.5% of the watershed's area is comprised of legacy sediment, and glacial deposits cover ~98% of the watershed (86% thin till, 14% thick till and coarse stratified deposits; MassGIS; Johnson, 2017; Fig. 2), and these deposits are likely to remain the dominant source, as erosion off of legacy exposures slows as the channel recovers from 18th-19th century human activity.

5.4 Mixing model limitations

Contributions estimated through the mixing model are subject to assumptions inherent in the model. Sediment transport dynamics are complex. The model assumes that all sediment is transported from each source equally, and does not account for grainsize effects. A high percentage of the glacial till matrix is silt and clay, and may have the ability to move farther in suspension. The legacy sediment is slightly coarser, composed of silt and fine sand, which could result in shorter distances travelled (Fig. 12). There are more opportunities for legacy sediment to be stored along the way in channel bars or on floodplains as it is coarser than glacial material (Fig. 12; Table 3), and there is more possibility for remobilization of this sediment after having previously been mobilized and stored. Storage of legacy sediment in these locations could reduce loads to the CED and result in an underestimation of the legacy contributions as a source of sediment during the 20th century.

Error in the model could draw contributions from the glacial and legacy sources each closer to 50%, which would be in proportion to their frequency of occurrence along the length of the channel (Fig. 3). However, as only two different bank sources and one tracer were used in the mixing model, it is likely that contributions for each of the two sources are overestimated. Sediment tracing studies in the Mid-Atlantic Piedmont suggest ~60% of sediment is eroding from the banks and ~40% is derived from upland hillslopes and agricultural land (Gellis et al., 2009; Mukundan et al., 2010) This model does not take into account additional sources, such as erosion of hillslope soil. Incorporating additional source types into the model might result in more representative contribution estimates, however, hillslope sediment is primarily developed from till, and would likely

be similar geochemically to other glacial sources. Only incorporating adjacent channel banks and glacial exposures is a reasonable first attempt, as they are the most proximal source to the channel, and directly release sediment into it.

Additional Hg analyses on active sediment in the channel could also be used to establish a record for concentrations of currently transported sediment and evaluate contributions of remobilized sediment to further evaluate timescale response. It could also provide information of Hg concentrations of mobilized sediment after the CED was filled in 1981. Only two samples obtained were fine grained enough to be evaluated for Hg (8-9 ppb; Table 5), suggesting lower erosion from mill ponds in the 21st century, and within the range of concentrations in the CED post 1953 (Fig. 9). However, more samples are necessary for a statistically robust dataset. Using additional geochemical tracers to create a composite mixing model would also categorize and distinguish different sediment sources more accurately, providing a more holistic representation of sediment contributions.

6. Conclusions

Overall, legacy deposits are a significant source of the sediment deposited behind the CED, despite only covering ~1.5% of the watershed area. Erosion from these deposits with high Hg concentrations was higher during the early 20th century, likely as a result of mill dam breaching releasing a pulse of sediment. This was followed by an increase in the relative contribution of erosion from glacial deposits, as represented by a decrease in Hg in the CED cores in the late 20th century. These findings suggest that there is a short recovery timescale response from this 18th- 19th perturbation during the first half of the

20th century, before returning to the more dominant long-term erosion signal from glacial material, consistent with processes observed at dam removal sites (Pearson et al., 2011; Sawaske and Fryeburg, 2012; Major et al., 2017). This trend is consistent with the pattern of high sedimentation rates to the CED early in the 20th century and lower sedimentation rates at the end of the century in Dow (2014; Fig. 8).

While much is yet to be known about how Hg cycles in the environment and how concentrations vary in upland sites in New England, it was effectively used as a tracer to distinguish the different source types in the South River watershed. Additional work on more accurately quantifying estimates from different source types could be accomplished through further analyses on the geochemistry of sediment. Identifying additional tracers, such as C or N isotopes related to agricultural activity, or using different instrumentation to identify trace metals could be used to develop a composite fingerprint to more accurately represent the source types for a more detailed mixing model. In addition, incorporating additional sources such as hillslopes and active channel deposits would result in a more holistic representation of contributions from different sources from the entire watershed to the CED.

GIS analyses indicate that the channel is not significantly widening along any section. The glacial reaches may be undergoing narrowing, however, this is probably highly influenced by the quality of the aerial imagery. While the legacy reaches are not changing significantly in width over the second half of the 20th century, they are exhibiting changes in sinuosity, suggesting that they are active sources of erosion, and that these deposits have contributed legacy sediment to the CED through the 20th century. Changes in channel width prior to the earliest available aerial photographs (1940) cannot

be evaluated, however, the mixing model suggests widening of legacy reaches may have occurred during this period, as dams breached. Further work comparing channel changes using repeat aerial imagery over the past several decades could be used to calculate trends in channel width changes and sinuosity during the second half of the 20th century.

Identifying sources of sediment in a watershed and quantifying erosion can help to guide river restoration practices. Direct field measurements, such as terrestrial LiDAR surveys, to quantify bank erosion would provide quantitative estimates on lateral migration of the banks, and could put erosion of New England legacy sediment into context with measured rates of bank erosion in the Mid-Atlantic region (Merritts et al., 2011; Lyons, 2015). Understanding fluvial readjustment to perturbations related to human land use compared to background erosion rates can inform timescale response to different events. This is especially important in New England because restoration practices developed in the Mid-Atlantic region and other unglaciated parts of the world may not be effective or the right choice for this formerly glaciated landscape. Overall, New England watersheds appear to display a resilience to anthropogenic disturbances over the past few hundred years, as erosion of legacy sediment only dominated the South River sediment load for the first half of the 20th century, although it does remain an important sediment source. Further work must be done to completely understand the full response timescale to the complete removal of legacy sediment from the system.

References

Ambers, R.K., 2001, Using the sediment record in a western Oregon flood-control reservoir to assess the influence of storm history and logging on sediment yield: Journal of Hydrology, v. 244, no. 3, p. 181-200.

Ballantyne, C.K., 2002, A general model of paraglacial landscape response: The Holocene, v. 12, no. 3, p. 371-376.

Banks, W., Gellis, A., and Noe, G., 2010, Sources of fine-grained suspended sediment in Mill Stream Branch watershed, Corsica River Basin, a tributary to the Chesapeake Bay, Maryland, 2009: Proceedings of the 2nd Joint Federal Interagency, Las Vegas, NV, v. 27.

Barten, D., and Kantor P., 2013, A River Runs Through Conway [Powerpoint slides]. Retrieved from http://www.friendsofthesouthriver.org/wpcontent/uploads/2013/03/RiverTalk_March 2013_updated.pdf.

Belmont, P., Willenbring, J.K., Schottler, S.P., Marquard, J., Kumarasamy, K., and Hemmis, J.M., 2014, Toward generalizable sediment fingerprinting with tracers that are conservative and nonconservative over sediment routing timescales: Journal of soils and sediments, v. 14, no. 8, p. 1479-1492.

Bierman, P., Lini, A., Zehfuss, P., Church, A., Davis, P.T., Southon, J., and Baldwin, L., 1997, Postglacial ponds and alluvial fans: Recorders of Holocene landscape history: GSA TODAY, v. 7, no. 10.

Blott, S.J., and Pye, K., 2001, GRADISTAT: a grain size distribution and statistics package for the analysis of unconsolidated sediments: Earth Surface Processes and Landforms, v. 26, no. 11, p. 1237-1248.

Brugam, R.B., 1978, Pollen indicators of land-use change in southern Connecticut: Quaternary Research, v. 9, no. 3, p. 349-362.

Collins, A., Walling, D., and Leeks, G., 1998, Use of composite fingerprints to determine the provenance of the contemporary suspended sediment load transported by rivers: Earth Surface Processes and Landforms, v. 23, no. 1, p. 31-52.

Collins, A., Walling, D., Webb, L., and King, P., 2010, Apportioning catchment scale sediment sources using a modified composite fingerprinting technique incorporating property weightings and prior information: Geoderma, v. 155, no. 3, p. 249-261.

Collins, M.J., Snyder, N.P., Boardman, G., et al., 2017, Channel response to sediment release: insights from a paired analysis of dam removal: Earth Surface Processes and Landforms.

Costa, J.E., 1975, Effects of agriculture on erosion and sedimentation in the Piedmont Province, Maryland: Geological Society of America Bulletin, v. 86, no. 9, p. 1281-1286.

Dean Jr, W.E., 1974, Determination of carbonate and organic matter in calcareous sediments and sedimentary rocks by loss on ignition: comparison with other methods: Journal of Sedimentary Research, v. 44, no. 1.

Dethier, E., Magilligan, F.J., Renshaw, C.E., and Nislow, K.H., 2016, The role of chronic and episodic disturbances on channel–hillslope coupling: the persistence and legacy of extreme floods: Earth Surface Processes and Landforms, v. 41, no. 10, p. 1437-1447.

Donovan, M., Miller, A., and Baker, M., 2016, Reassessing the role of milldams in Piedmont floodplain development and remobilization: Geomorphology, v. 268, p. 133-145.

Dow, S., 2014, Sedimentation behind Conway Electric Dam, South River, western Massachusetts [B.A. thesis]: University of Connecticut, 55 p.

Duruibe, J., Ogwuegbu, M., and Egwurugwu, J., 2007, Heavy metal pollution and human biotoxic effects: International Journal of Physical Sciences, v. 2, no. 5, p. 112-118.

Edwards, B.F., and Smith, D.H., 2002, River meandering dynamics: Physical Review E, v. 65, no. 4, p. 046303.

Emerson, B. K., 1898, Geology of old Hampshire county, Massachusetts comprising Franklin, Hampshire, and Hampden counties: Washington, Government Printing Office, Monographs of the United States Geologic Survey, v. 29, 782 p.

Field, J., 2013, Fluvial Geomorphic Assessment of the South River Watershed, MA: Unpublished report prepared for Franklin Regional Council of Governments Greenfield MA on behalf of Field Geology Services, 108 p.

Flanders, J., Turner, R., Morrison, T., Jensen, R., Pizzuto, J., Skalak, K., and Stahl, R., 2010, Distribution, behavior, and transport of inorganic and methylmercury in a high gradient stream: Applied Geochemistry, v. 25, no. 11, p. 1756-1769.

Foster D, Motzkin G., 2009, 1830 Map of Land Cover and Cultural Features in
Massachusetts: Harvard Forest Data Archive: HF122.

Galster, J.C., Pazzaglia, F.J., and Germanoski, D., 2008: Measuring the Impact of
Urbanization on Channel Widths Using Historic Aerial Photographs and Modern
Surveys.

Graf, W.L., 1999, Dam nation: A geographic census of American dams and their large-
scale hydrologic impacts: Water Resources Research, v. 35, no. 4, p. 1305-1311.

Gellis, A.C., Hupp, C.R., Pavich, M.J., Landwehr, J.M., Banks, W.S.L., Hubbard, B.E.,
Langland, M.J., Ritchie, J.C., Reuter, J.M., 2009. Sources, transport, and storage of
sediment at selected sites in the Chesapeake Bay watershed. U.S. Geological Survey
Scientific Investigations Report 2008-5186, 95 ppFrancis, D.R., and Foster, D.R.,
2001, Response of small New England ponds to historic land use: The Holocene, v.
11, no. 3, p. 301-312.

Haddadchi, A., Ryder, D.S., Evrard, O., and Olley, J., 2013, Sediment fingerprinting in
fluvial systems: review of tracers, sediment sources and mixing models:
International Journal of Sediment Research, v. 28, no. 4, p. 560-578.

Hooke, R. LeB., 1994, On the efficacy of humans as geomorphic agents: GSA Today, v.
4, no. 9, p. 217, 224–225.

Horowitz, A.J., and Elrick, K.A., 1987, The relation of stream sediment surface area,
grain size and composition to trace element chemistry: Applied Geochemistry, v. 2,
no. 4, p. 437-451.

Howes, F. G., 1910, A History of the Town of Ashfield Franklin County, Massachusetts
from its Settlement in 1742 to 1910: Ashfield, MA, Town of Ashfield, 425 p.

Jacobson, R.B., and Coleman, D.J., 1986, Stratigraphy and recent evolution of Maryland
Piedmont flood plains: American Journal of Science, v. 286, no. 8, p. 617-637.

Jackson, M., and Roering, J.J., 2009, Post-fire geomorphic response in steep, forested
landscapes: Oregon Coast Range, USA: Quaternary Science Reviews, v. 28, no. 11,
p. 1131-1146.

James, A., 1999, Time and the persistence of alluvium: River engineering, fluvial
geomorphology, and mining sediment in California: Geomorphology, v. 31, no. 1, p.
265-290.

James, A., 2013: Legacy sediment: Definitions and processes of episodically produced anthropogenic sediment. Anthropocene 2, 16–26.

Johnson, K. M., 2017, Quantifying milldam legacy sediment storage in valley bottoms of two New England watersheds [M.S. thesis]: Boston College.

Kamman, N.C., and Engstrom, D.R., 2002, Historical and present fluxes of mercury to Vermont and New Hampshire lakes inferred from 210 Pb dated sediment cores: Atmospheric Environment, v. 36, no. 10, p. 1599-1609.

Korup, O., McSaveney, M.J., and Davies, T.R., 2004, Sediment generation and delivery from large historic landslides in the Southern Alps, New Zealand: Geomorphology, v. 61, no. 1, p. 189-207.

Lamborg, C.H., Fitzgerald, W.F., Skoog, A., and Visscher, P.T., 2004, The abundance and source of mercury-binding organic ligands in Long Island Sound: Marine Chemistry, v. 90, no. 1, p. 151-163.

Lindqvist, O., and Rodhe, H., 1985, Atmospheric mercury-a review*: Tellus B, v. 37, no. 3.

Lyons, N.J., Starek, M.J., Wegmann, K.W., and Mitasova, H., 2015, Bank erosion of legacy sediment at the transition from vertical to lateral stream incision: Earth Surface Processes and Landforms, v. 40, no. 13, p. 1764-1778.

Mabit, L., Benmansour, M., and Walling, D., 2008, Comparative advantages and limitations of the fallout radionuclides 137 Cs, 210 Pb ex and 7 Be for assessing soil erosion and sedimentation: Journal of environmental radioactivity, v. 99, no. 12, p. 1799-1807.

Major, J. J., A. E. East, J. E. O'Connor, G. E. Grant, A. C. Wilcox, C. S. Magirl, M. J. Collins, and D. D. Tullos (2017), Geomorphic response to U.S. Dam Removals—A two-decade perspective, in *Gravel-Bed Rivers: Processes and Disasters*, edited by D. Tsutsumi and J. Laronne, pp. 355–383, Wiley and Sons.

MassGIS, 2015, Surficial Geology (1: 24,000), ttp://www.mass.gov/anf/research-and-tech/it-serv-and-support/application-serv/office-of-geographic-information-massgis/datalayers/sg24k.html.

Mazzullo, J., Ehrlich, R., and Hemming, M.A., 1984, Provenance and areal distribution of late Pleistocene and Holocene quartz sand on the southern New England continental shelf: Journal of Sedimentary Research, v. 54, no. 4.

McLennan, S., Bock, B., Compston, W., Hemming, S., and McDaniel, D., 2001, Detrital zircon geochronology of Taconian and Acadian foreland sedimentary rocks in New England: Journal of Sedimentary Research, v. 71, no. 2, p. 305-317.

Merritts, D., Walter, R., Rahnis, M., et al., 2011, Anthropocene streams and base-level controls from historic dams in the unglaciated mid-Atlantic region, USA: Philosophical transactions.Series A, Mathematical, physical, and engineering sciences, v. 369, no. 1938, p. 976-1009.

Merritts, D., Walter, R., Rahnis, M., et al., 2013, The rise and fall of Mid-Atlantic streams: Millpond sedimentation, milldam breaching, channel incision, and stream bank erosion: Reviews in Engineering Geology, v. 21, p. 183-203.

Miller, J. R., Mackin, G., and Miller, S. M.O., 2015, Application of Geochemical Tracers to Fluvial Sediment: New York, Springer, 141 p.

Milliman, J.D., and Syvitski, J.P., 1992, Geomorphic/tectonic control of sediment discharge to the ocean: the importance of small mountainous rivers: The Journal of geology, p. 525-544.

Mukundan, R., Radcliffe, D., Ritchie, J., Risse, L., and McKinley, R., 2010, Sediment fingerprinting to determine the source of suspended sediment in a southern Piedmont stream: Journal of environmental quality, v. 39, no. 4, p. 1328-1337.

Mukundan, R., Walling, D.E., Gellis, A.C., Slattery, M.C., and Radcliffe, D.E., 2012: Sediment Source Fingerprinting: Transforming From a Research Tool to a Management Tool.

Niemitz, J., Haynes, C., and Lasher, G., 2013, Legacy sediments and historic land use: Chemostratigraphic evidence for excess nutrient and heavy metal sources and remobilization: Geology, v. 41, no. 1, p. 47-50.

Noller, J. S., Sowers, J. M., and Lettis, W.R., 2000, Quarternary Geochronology: Methods and Applications: Washington DC, American Geophysical Union, 582 p.

Nriagu, J.O., and Pacyna, J.M., 1988, Quantitative assessment of worldwide contamination of air, water and soils by trace metals: Nature, v. 333, no. 6169, p. 134-139.

Office of Geographic Information (MassGIS), 2009. Commonwealth of Massachusetts, MassIT.

Pacyna, J.M., and Pacyna, E.G., 2001, An assessment of global and regional emissions of trace metals to the atmosphere from anthropogenic sources worldwide: Environmental Reviews, v. 9, no. 4, p. 269-298.

Palazón, L., Gaspar, L., Latorre, B., Blake, W.H., and Navas, A., 2015, Identifying sediment sources by applying a fingerprinting mixing model in a Pyrenean drainage catchment: Journal of Soils and Sediments, v. 15, no. 10, p. 2067-2085.

Pearson, A.J., Snyder, N.P., and Collins, M.J., 2011, Rates and processes of channel response to dam removal with a sand-filled impoundment: Water Resources Research, v. 47, no. 8.

Pease, C. S. (Ed.), 1917, History of Conway (Massachusetts) 1767-1917: Springfield, MA, Springfield Printing and Binding Company, 345 p.

Peizhen, Z., Molnar, P., and Downs, W.R., 2001, Increased sedimentation rates and grain sizes 2-4 Myr ago due to the influence of climate change on erosion rates: Nature, v. 410, no. 6831, p. 891.

Perry, E., Norton, S.A., Kamman, N.C., Lorey, P., and Driscoll, C.T., 2005, Deconstruction of historic mercury accumulation in lake sediments, northeastern United States: Ecotoxicology, v. 14, no. 1-2, p. 85-99.

Pizzuto, J., 2002, Effects of Dam Removal on River Form and Process: Although many well-established concepts of fluvial geomorphology are relevant for evaluating the effects of dam removal, geomorphologists remain unable to forecast stream channel changes caused by the removal of specific dams: AIBS Bulletin, v. 52, no. 8, p. 683-691.

Pizzuto, J., and O'Neal, M., 2009, Increased mid-twentieth century riverbank erosion rates related to the demise of mill dams, South River, Virginia: Geology, v. 37, no. 1, p. 19-22.

Pizzuto, J., Skalak, K., Pearson, A., and Benthem, A., 2016, Active overbank deposition during the last century, South River, Virginia: Geomorphology, v. 257, p. 164-178.

Renwick, W., Smith, S., Bartley, J., and Buddemeier, R., 2005, The role of impoundments in the sediment budget of the conterminous United States: Geomorphology, v. 71, no. 1, p. 99-111.

Reusser, L., Bierman, P., and Rood, D., 2015, Quantifying human impacts on rates of erosion and sediment transport at a landscape scale: Geology, v. 43, no. 2, p. 171-174.

Rhoades, E.L., O'Neal, M.A., and Pizzuto, J.E., 2009, Quantifying bank erosion on the South River from 1937 to 2005, and its importance in assessing Hg contamination: Applied Geography, v. 29, no. 1, p. 125-134.

Sawaske, S.R., and Freyberg, D.L., 2012, A comparison of past small dam removals in highly sediment-impacted systems in the US: Geomorphology, v. 151, p. 50-58.

Schenk, E.R., and Hupp, C.R., 2009, Legacy Effects of Colonial Millponds on Floodplain Sedimentation, Bank Erosion, and Channel Morphology, Mid-Atlantic, USA: JAWRA Journal of the American Water Resources Association, v. 45, no. 3, p. 597-606.

Small, I.F., Rowan, J.S., and Franks, S.W., 2002, Quantitative sediment fingerprinting using a Bayesian uncertainty estimation framework: International Association of Hydrological Sciences, Publication, v. 276, p. 443-450.

Stone, J.R., and DiGiacomo-Cohen, M.L., comps., 2010, Surficial geologic map of the Heath-Northfield-Southwick-Hampden 24-quadrangle area in the Connecticut Valley region, west-central Massachusetts: U.S. Geological Survey Open-File Report 2006-1260-G.

Stout, J.C., and Belmont, P., 2014, TerEx Toolbox for semi-automated selection of fluvial terrace and floodplain features from lidar: Earth Surface Processes and Landforms, v. 39, no. 5, p. 569-580.

Syvitski, J.P., Vorosmarty, C.J., Kettner, A.J., and Green, P., 2005, Impact of humans on the flux of terrestrial sediment to the global coastal ocean: Science (New York, N.Y.), v. 308, no. 5720, p. 376-380.

Thorson, R.M., Harris, A.G., Harris, S.L., Gradie, R., and Lefor, M., 1998, Colonial impacts to wetlands in Lebanon, Connecticut: Reviews in Engineering Geology, v. 12, p. 23-42.

United States Geological Survey (USGS), 2017, USGS current water data for the USA: https://waterdata.usgs.gov/nwis/rt (accessed July 2017).

Varekamp, J., Kreulen, B., Buchholtz, M., and Mecray, E., 2003, Mercury contamination chronologies from Connecticut wetlands and Long Island Sound sediments: Environmental Geology, v. 43, no. 3, p. 268-282.

Varekamp, J.C., 2006, The historic fur trade and climate change: Eos, Transactions American Geophysical Union, v. 87, no. 52, p. 593-597.

Walling, D.E., 2004, Using environmental radionuclides to trace sediment mobilization and delivery in river basins as an aid to catchment management, *in* Proceedings of the Ninth International Symposium on River Sedimentation, p. 18-21.

Walling, D., 2005, Tracing suspended sediment sources in catchments and river systems: Science of the total environment, v. 344, no. 1, p. 159-184.

Walling, D., 2006, Human impact on land–ocean sediment transfer by the world's rivers: Geomorphology, v. 79, no. 3, p. 192-216.

Walter, R.C., and Merritts, D.J., 2008, Natural streams and the legacy of water-powered mills: Science (New York, N.Y.), v. 319, no. 5861, p. 299-304.

Wilkinson, B.H., and McElroy, B.J., 2007, The impact of humans on continental erosion and sedimentation: Geological Society of America Bulletin, v. 119, no. 1-2, p. 140-156.

Woodruff, J.D., Martini, A.P., Elzidani, E.Z., Naughton, T.J., Kekacs, D.J., and MacDonald, D.G., 2013, Off-river waterbodies on tidal rivers: Human impact on rates of infilling and the accumulation of pollutants: Geomorphology, v. 184, p. 38-50.

Zapata, F., 2003, The use of environmental radionuclides as tracers in soil erosion and sedimentation investigations: recent advances and future developments: Soil and Tillage Research, v. 69, no. 1, p. 3-13.

Table 1. Land use in the town of Conway.

Category	1830^	1920^	1952*	1971**	1985**	1999**	2005**
Forested	21%	58%	79%	84%	83%	82%	84%
Agriculture	77%	40%	20%	12%	12%	11%	8%
Other	2%	3%	1%	4%	5%	7%	8%

^Data from Harvard forest GIS shapefiles.

*USGS land sheets from UMass Amherst corresponding with aerial photographs.

**Town stats from MassGIS website interpreted from 1:25000 aerial photography.

Table 2. Land use in the town of Ashfield.

Category	1830^	1920^	1971**	1985**	1999**	2005**
Forested	7%	56%	81%	80%	80%	81%
Agriculture	91%	43%	13%	12%	10%	7%
Other	2%	1%	6%	8%	10%	13%

^Data from Harvard forest GIS shapefiles.
**Town stats from MassGIS website interpreted from 1:25000 aerial photography.

Table 3. Grainsizes for the four mill pond sites as average D50 (µm).

Sample location	Average D_{50} (µm)	D_{50} 1σ range (µm)	# of samples
MPSR1	142	52-386	18
MPSR2	185	79-430	19
MPSR4	144	110-189	17
MPSR5	101	47-222	14

Table 4. Average Hg concentrations for glacial, mill pond, and Conway Electric Dam vibracore (VC3 and VC5) samples. Note: the Conway Electric Dam combines VC3 and VC5.

Sample location	Average Hg (ppb)	Log transformed average	Converted average (Hg in ppb)	Error 1σ range	# of samples
Glacial	2.22 ± 0.96	0.31 ± 0.18	2.06	1.37 - 3.08	11
Mill Pond	32.37 ± 70.64	1.13 ± 0.50	13.36	4.19 - 42.60	57
VC3	7.52 ± 4.39	0.81 ± 0.28	6.30	3.31 - 11.98	21
VC5	18.21 ± 10.13	1.20 ± 0.22	15.99	9.60 - 26.63	30
Conway Electric Dam	13.81 ± 9.77	1.03 ± 0.32	10.89	5.26 - 22.58	51

Table 5. Percent organics, grainsize, and Hg concentrations for active channel samples taken from the bed of the South River.

Sample	% organic	% fine	D50 (um)	Hg (ppb)
MPSR1_A	2.00	8.81	20.6	8.41
MPSR1_M	5.85	20.24	113.8	9.36
MPSR1_A2	0.91	2.34	311.5	-
MPSR2_A	1.77	5.31	609.9	-
MPSR4_A	0.84	0.91	850.7	-
MPSR5_A	3.10	14.05	372.1	-

Table 6. ^{137}Cs and ^{210}Pb concentrations measured in mill pond sediment. Error is reported to 1σ.

Site	Depth (cm)	^{137}Cs (Bq/kg)	^{210}Pb (Bq/kg)
MPSR1	15	12.3 ± 0.56	82.94 ± 14.25
MPSR1	100	0 ± 0.00	90.33 ± 25.81
MPSR1	170	0 ± 0.00	66.91 ± 14.48
MPSR2	10	1.61 ± 0.35	58.51 ± 9.24
MPSR2	20	3.83 ± 0.39	59.21 ± 38.50
MPSR2	30	15.76 ± 0.88	49.21 ± 8.86
MPSR2	40	0.61 ± 0.37	42.89 ± 6.26
MPSR2	90	0 ± 0.00	44.36 ± 17.11
MPSR2	170	0 ± 0.00	39.97 ± 7.87
MPSR4	20	0 ± 0.00	55.19 ± 29.92
MPSR4	120	0 ± 0.00	51.31 ± 69.71
MPSR4	180	0 ± 0.00	42.38 ± 6.52
MPSR5	20	4.73 ± 0.46	76.02 ± 11.83
MPSR5	120	0 ± 0.00	37.15 ± 6.06
MPSR5	180	0 ± 0.00	45.07 ± 6.78

Table 7. XRF data for glacial sediment. LOD stands for level of detection.

Sample	Zr	Sr	Rb	Th	As	Zn	Cu	Fe	Mn	Cr	V	Ti	Sc	Ca	K
RBR1	193.71	131.6	64.92	12.76	3.59	67.93	10.91	30140.43	534.18	66.36	130.76	4272.91	24.7	14090.17	28512.65
RBR3	211.22	143.35	76.62	9	< LOD	62.73	16.44	30536.96	509.22	75.14	162.87	4662.56	19.3	15520.89	30376.84
MM2	152.64	138.14	64.06	8.37	< LOD	65.68	19.17	29992.01	770.39	50.26	140.01	5480.73	14.12	8727.78	26316.27
SP2	113.48	68.37	23.74	< LOD	< LOD	31.75	< LOD	23584.48	310.82	< LOD	108.56	7372.71	14.01	13048.79	19434.8

Table 8. XRF data for elements detected in some but not all glacial and legacy sediment samples. LOD stands for level of detection. MPSR samples are from legacy sediment, the last four samples are glacial.

Sample	Mo	Th	Pb	Cu	Cr	S
Legacy						
MPSR2_10	5.72	5.65	< LOD	< LOD	28.67	211.35
MPSR2_20	< LOD	4.11	< LOD	< LOD	15.08	< LOD
MPSR2_40	4.65	< LOD	< LOD	< LOD	< LOD	213.85
MPSR2_50	< LOD	4.99	4.33	< LOD	23.36	< LOD
MPSR2_60	< LOD	< LOD	< LOD	< LOD	< LOD	242.76
MPSR2_70	< LOD	5.26	< LOD	< LOD	25.08	< LOD
MPSR2_80	< LOD	2.92	< LOD	< LOD	24.62	< LOD
MPSR2_90	< LOD	3.05	< LOD	< LOD	< LOD	< LOD
MPSR2_100	< LOD	< LOD	< LOD	< LOD	20.6	< LOD
MPSR2_110	< LOD	< LOD	< LOD	< LOD	< LOD	< LOD
MPSR2_120	< LOD	< LOD	< LOD	< LOD	27.48	< LOD
MPSR2_130	< LOD	5.3	< LOD	< LOD	43.21	< LOD
MPSR2_140	3.3	< LOD	< LOD	< LOD	< LOD	< LOD
MPSR2_150	< LOD	5.56	< LOD	< LOD	35.48	< LOD
MPSR2-160	2.26	< LOD	< LOD	< LOD	< LOD	< LOD
MPSR2_170	< LOD	6.5	< LOD	< LOD	46.58	< LOD
MPSR2_180	< LOD	< LOD	< LOD	< LOD	25.38	< LOD
MPSR2_190	< LOD	< LOD	< LOD	< LOD	17.54	< LOD
Glacial						
RBR1	< LOD	12.76	< LOD	10.91	66.36	< LOD
RBR3	< LOD	9	< LOD	16.44	75.14	< LOD
MM2	< LOD	8.37	< LOD	19.17	50.26	< LOD
SP2	< LOD	< LOD	< LOD	< LOD	< LOD	< LOD

Table 9. XRF data for elements detected in core VC5. Elements that were not detected at any depth are not shown (Se, Au, W, Cd, Ag, Pd).

Depth (cm)	Mo	Zr	Sr	U	Rb	Th	Pb	As	Zn	Cu	Ni	Fe	Mn
10	3.08	188.12	137.96	0	50.8	4.98	0	0	67.05	0	0	26607	575
20	0	171.18	121.59	0	35.78	3.62	0	0	47.61	0	0	24374	336.93
30	4.18	270.51	181.4	0	72.33	8.79	12.75	0	79.97	0	0	30969	739.08
40	0	199.85	136.18	0	55.17	7	6.38	0	73.17	0	0	29278	745.65
50	0	306.51	190.81	6.69	73.31	11.1	11.37	6.03	85.62	18.06	0	31034	785.84
60	0	311.93	178.57	6.26	81.23	10.28	19.88	0	97.24	18.93	0	34408	745.73
70	0	285.74	182.19	0	78.73	9.17	15.15	4.41	79.11	19.06	0	29493	599.89
80	0	182.85	154	6	46.26	6.85	9.99	0	56.18	0	0	22608	467.94
90	0	218.3	172.05	0	56.28	6.32	10.28	4.39	70.96	0	0	25691	520.17
100	0	201.12	145.56	6.01	53.28	7.61	9.04	0	59.86	0	0	24584	407.52
110	0	256.52	150.28	0	46.42	7.87	7.03	0	56.92	0	0	22853	433.97
120	0	221.13	165.75	0	54.67	8.97	6.34	0	59.74	0	0	24955	518.13
130	0	263.61	105.69	0	37.94	7.88	10.58	0	60.11	0	43.59	37624	1455.66
140	0	138.58	145.42	0	38.54	5.82	0	0	52.07	13.15	51.6	24008	659.55
150	0	151.53	143.07	0	39.97	5.1	0	3.91	52.1	0	28.59	21322	491.47
160	0	197.86	171.21	8.22	69.1	8.97	8.94	0	71.45	0	36.67	26957	536.89
170	0	156.66	148.08	0	39.58	5.98	0	0	51.88	0	0	22651	481.02
180	0	145.56	129.66	0	29.34	5	0	0	43.18	0	0	17904	487.84
190	0	209.59	146.42	0	46.16	6.63	9.18	0	60.55	12.01	0	26787	639.29
200	0	170.9	135.05	6.96	39.76	8.26	0	3.85	50.93	12.63	27.68	21935	572.42
210	0	185.13	148.4	6.34	45.89	8.08	7.25	0	60.68	0	26.68	24394	591.38
220	0	267.96	195.48	7.96	77.55	7.98	14.59	0	76.53	16.77	0	28069	560.13
230	0	275.09	189.26	9.4	86.08	10.46	14.17	0	85.02	0	0	37003	918.92
240	0	357.56	194.43	8.85	119.6	14.5	20.45	0	107.96	27.48	0	36513	677.27
250	0	300.1	188.48	7.7	109.82	11.35	14.7	0	83.91	18.41	0	35857	797.29
260	0	99.73	162.76	0	34.31	9.29	0	0	45.21	0	0	22936	631.78
270	2.98	125.39	137.15	0	37.37	5.12	0	0	49.11	0	0	22966	569.41
280	0	69.17	115.03	4.5	27.1	3.91	0	0	41.2	0	0	19084	395.97
290	0	287.69	172.91	6.46	77.47	9.14	15.43	0	78.03	13.05	0	29268	633.72
300	3.37	246.09	170.62	0	69.44	9.45	26.59	5.8	107.11	29.78	0	33311	780.22
310	6.22	128.53	120.71	0	30.64	3.39	0	0	51.05	0	0	25028	560.44
320	0	237.16	170.89	0	68.08	9.35	28.57	6.66	114.91	20.86	0	33173	565.83
330	6.73	138.71	141.93	5.28	43.23	6.15	9.85	0	70.95	0	0	25145	400.87
340	0	111.54	116.49	0	31.75	4.19	0	0	44.5	0	0	19641	454.32
345	3.18	141.67	130.64	7.58	44.95	5.19	16.86	0	75.45	0	0	25752	479.43
350	0	132.67	124.34	U	42.41	6.97	8.81	4.93	57.93	0	Ni	23576	522.65
360	0	225.53	155.52	8.83	55.69	6.08	15.41	0	87.43	0	0	29229	571.14
370	3.94	114.83	136.82	0	41.96	4.13	8.68	0	59.06	0	0	20971	329.24
380	0	215.28	170	5.69	66.82	9.19	25.9	0	93.25	13.17	0	29075	574.88
390	0	243.1	165.27	0	69.19	10.9	18.95	5.64	100.22	0	0	31395	630.21
400	0	127.86	120.12	0	42.91	3.83	0	0	47.33	12.74	0	19396	367.04
410	6.39	120.12	123.98	0	41.63	4.67	9.89	0	71.04	0	0	25474	482.95
420	0	236.18	142.82	0	74.87	8.95	36.15	0	121.16	20.12	0	34994	862.07
430	0	187.66	142.47	0	55.87	5.62	4.79	3.87	61.15	12.74	0	25944	549.15
440	0	108.75	139.03	0	36.92	7.37	0	0	45.06	0	0	18337	439.11
450	0	135.11	120.81	0	31.98	4.77	0	0	67.8	0	0	22494	535.39
460	0	137.42	125.13	0	39.94	3.16	4.22	0	57.72	0	0	22734	517.75
470	0	154.25	131.42	0	54.28	3.75	8.33	0	75.75	0	0	22409	415.63
480	0	186.63	124.81	0	69.78	8	17.81	5.09	97.04	11.28	0	31928	605.57
490	2.46	110.97	121.85	4.93	48.2	4.74	5.82	0	62.89	0	0	28546	699.45

(Table 9 cont.)

Depth (cm)	Cr	V	Ti	Sc	Ca	K	S	Ba	Cs	Te	Sb	Sn	Hg	Co
10	34.85	112.56	5390.42	26.13	14347	19102.31	0	0	0	0	0	0	0	0
20	29.82	69.74	2216.22	8.53	7131.4	10700.85	0	0	0	0	0	0	0	0
30	39.65	112.63	4589.93	15.88	12113	16468.93	0	0	0	0	0	0	6.19	0
40	47.78	107.64	4609.24	18.55	12488	17978.94	0	0	0	0	0	0	0	0
50	51.44	100.17	4269.01	24.77	12048	16397.22	0	206.99	0	0	0	0	0	0
60	56.84	121.54	4634.37	19.99	11503	19156.2	220.31	59	0	0	0	0	0	117.45
70	49.26	113.43	4367.44	12.33	11030	19688.03	0	135.02	0	0	0	0	0	0
80	28.36	64.47	4418.95	17.63	11056	11348.89	152	95.22	0	0	0	0	0	0
90	48.42	88.76	4628.58	19.59	11652	15240.33	295.19	0	0	0	0	0	0	0
100	38.41	99.78	4804.24	15.63	10830	16191.04	299.36	0	0	0	0	0	0	0
110	32.37	69.79	5189.59	11.88	11401	12048.58	151.78	102.9	0	0	0	0	0	0
120	45.93	96.98	4996.77	22.71	13080	15802.17	640.03	0	0	0	0	0	0	0
130	42.74	87.51	6102.52	26.24	13083	13319.96	0	171.28	21.58	0	0	68	0	0
140	39.67	89.7	4544.53	16.14	10819	15501.42	380.32	254.79	29.67	47.54	15.56	0	0	0
150	29.94	73.38	6777.32	28.67	15172	13794.92	0	130.57	0	0	0	0	0	0
160	45.43	89.4	4437.22	21.99	11781	17146.96	0	248.07	11.29	0	0	0	0	0
170	18.42	58.48	5304.72	16.01	11207	11187.74	0	165.39	11.34	0	0	0	0	0
180	0	52.02	5121.17	19.21	11615	7844.23	0	66.27	0	0	0	0	0	0
190	35.65	89.7	5772.62	12.93	10847	14621.64	190.66	62.98	0	0	0	0	0	0
200	35.81	80.32	4255.82	15.16	11244	14421.28	0	244.24	22.73	0	15.24	0	0	0
210	43.53	91.05	5703.86	25.69	10808	14928.94	0	242.93	16.68	0	0	0	0	0
220	45.49	102.96	4894.16	24.32	12682	18513.38	0	194.33	0	0	0	0	0	0
230	50.41	117.3	4792.19	21.96	11551	17646.86	0	0	0	0	0	0	0	0
240	75.61	144.48	4119.12	9.53	9206.2	24330.91	0	179.88	0	0	0	0	0	0
250	71.95	112.18	4145.92	16.95	9559.3	24161.54	0	105.25	0	0	0	0	0	0
260	16.03	55.61	3480.57	10.8	8715.4	11228.57	0	0	0	0	0	0	0	0
270	26.42	73.34	3979.7	14.43	8870.8	12374.59	0	0	0	0	0	0	0	0
280	21.71	38.48	3886.93	15.46	8663.6	7686.38	196.05	0	0	0	0	0	0	0
290	46.41	118.41	3831.22	21.34	11005	18386.55	0	0	0	0	0	0	0	0
300	49.94	97.39	4173.99	16.45	11304	14507.02	303.48	0	0	0	0	0	0	0
310	16.02	55.26	6641.36	17.3	12064	9253.98	177.96	0	0	0	0	0	0	0
320	51.36	112.93	4369	15.88	11044	15059.81	384.51	0	0	0	0	0	0	0
330	40.42	56.57	3643.84	12.49	9020.8	10878.93	310.2	0	0	0	0	0	0	0
340	27.09	54.24	3762.92	17.63	9667.5	8914.6	0	0	0	0	0	0	0	0
345	35.06	75.21	4257.86	16.3	10347	12775	168.81	0	0	0	0	0	0	0
350	25.64	56.35	4463.82	16.32	9942.4	9581.05	270.79	0	0	0	0	0	0	0
360	43.32	89.9	4404.38	17.03	10566	14095.12	273.03	0	0	0	0	0	0	0
370	16.86	68.42	3354.14	13.49	9237.9	9422.76	147.77	0	0	0	0	0	0	0
380	41.65	94.69	4369.13	20.71	10727	14108.47	309.9	0	0	0	0	0	0	0
390	48.75	98.08	4419.93	20.23	10355	16076.23	249.1	0	0	0	0	0	0	0
400	12.17	50.52	3743.11	15.84	8708.4	9867.15	0	0	0	0	0	0	0	0
410	33.04	63.03	2845.62	9.15	6993.7	9786.15	366.99	0	0	0	0	0	0	0
420	62.82	135.61	5708.26	23.44	13024	26026.96	385.06	0	0	0	0	0	0	0
430	52.2	107.44	6040.17	12.04	13484	20427.49	0	0	0	0	0	0	0	0
440	0	74.84	5889.87	12.94	10608	10073.35	0	0	0	0	0	0	0	0
450	31.06	67.4	7542.23	16.41	13132	10304.58	0	0	0	0	0	0	0	0
460	21.31	87.25	7441.27	22.5	15560	12889.64	209.48	0	0	0	0	0	0	0
470	32.38	123.47	5321.64	16.87	13469	19322.74	0	0	0	0	0	0	0	0
480	72.84	146.95	5529.18	20.13	12342	26399.21	498.04	0	0	0	0	0	0	0
490	44.42	117.66	4874.91	19.35	12415	19379.06	230.47	0	0	0	0	0	0	0

Table 10. Percent contributions of glacial and legacy sediment to the Conway Electric Dam.

Mixing model	Mill Hg conc. (ppb)	Glacial Hg conc. (ppb)	CED Hg conc. (ppb)	Glacial Contribution	Legacy Contribution
Entire deposit (VC3 & VC5)	13.36	2.06	10.89	32 ± 10 %	68 ± 10%
Pre-1953	13.36	2.06	11.33	26 ± 35 %	74 ± 35 %
Post-1953	13.36	2.06	8.84	63 ± 14 %	37 ± 14 %
Mixing model (sensitivity analysis)					
Entire deposit (VC3 & VC5)	11.84	2.06	10.89	15 ± 36%	85 ± 36%
Pre-1953	11.84	2.06	11.33	8 ± 40%	92 ± 40%
Post-1953	11.84	2.06	8.84	54 ± 15%	46 ± 15%

Table 11. Width changes and sinuosity for each reach (Figs. 11 and 25). Width change was calculated as 2014-1940. Sinuosity is calculated as the curvy distance of the stream divided by the straight distance of the valley for that section, calculated for both 1940 and 2014. P-values from the t-test for changes in channel width indicate reaches 5 and 6 show significant change.

Reach	Sediment type	1940 Sinuosity	2014 Sinuosity	Percent change	Width change (m)	Width change T-test p value
1	Glacial	1.39	1.40	1%	0 ± 4	0.7322
2	Legacy	1.43	1.43	0%	0 ± 5	0.6854
3	Glacial	1.51	1.54	2%	0 ± 4	0.8936
4	Legacy	1.08	1.21	12%	0 ± 3	0.9338
5	Glacial	1.52	1.53	1%	4 ± 6	**< 0.05**
6	Legacy	1.29	1.45	12%	3 ± 2	**< 0.05**
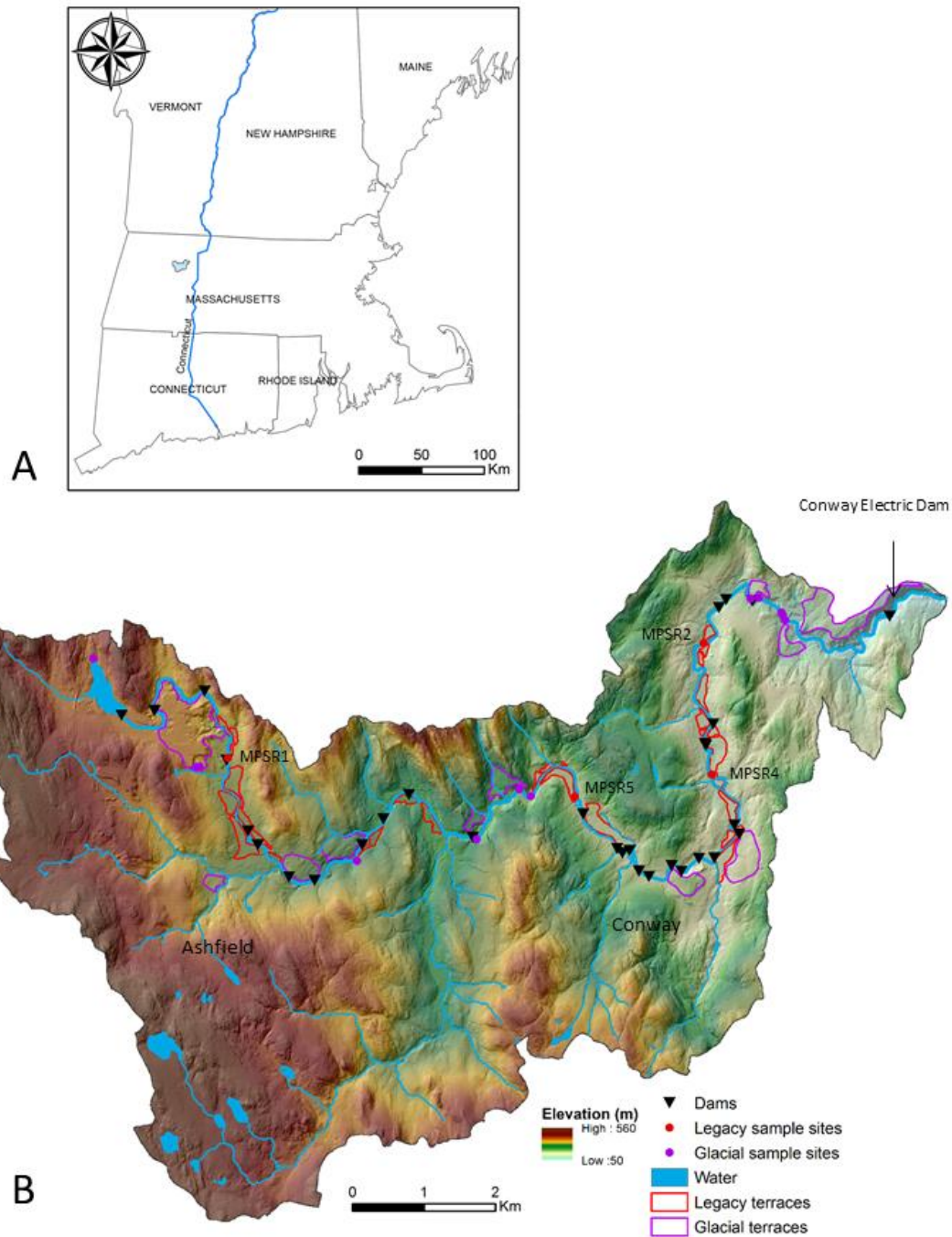
Figure 1. (A) Map of southern New England, displaying location of the South River watershed in western Massachusetts. (B) Location map of the South River watershed; base is 2 m LiDAR with hillshade overlay. Sampling sites of mill pond sediment (red circles) and glacial sediment (purple circles) are shown. Historic dams along the mainstem river are denoted by black triangles. Only dams and terraces along the mainstem channel are shown, as it is assumed that erosion of glacial and legacy sources is primarily occurring off of deposits adjacent to the mainstem channel.
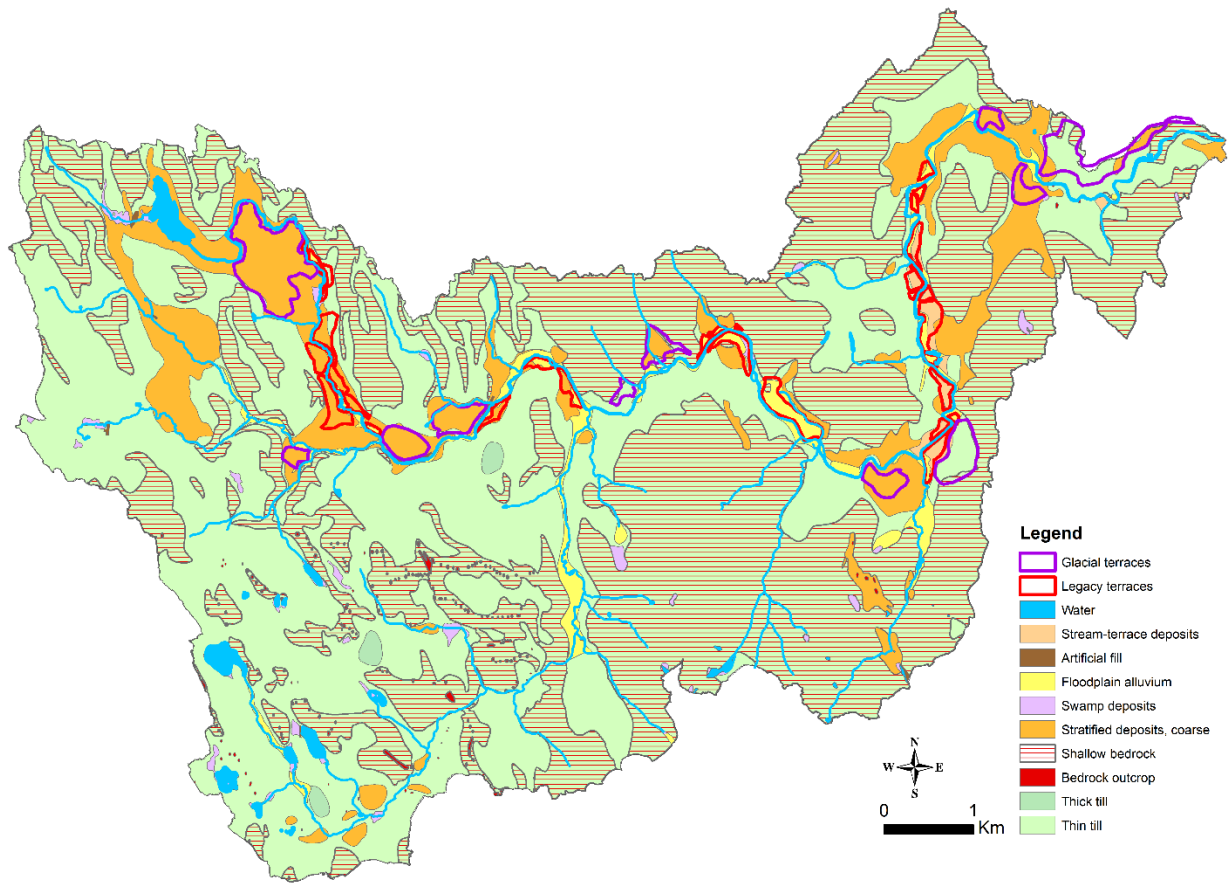
Figure 2. Map of surficial deposits in the South River watershed (original map scale 1:24,000; MassGIS, 2015). Legacy and glacial terraces mapped using TerEx, LiDAR features, and field observations (Johnson, 2017).
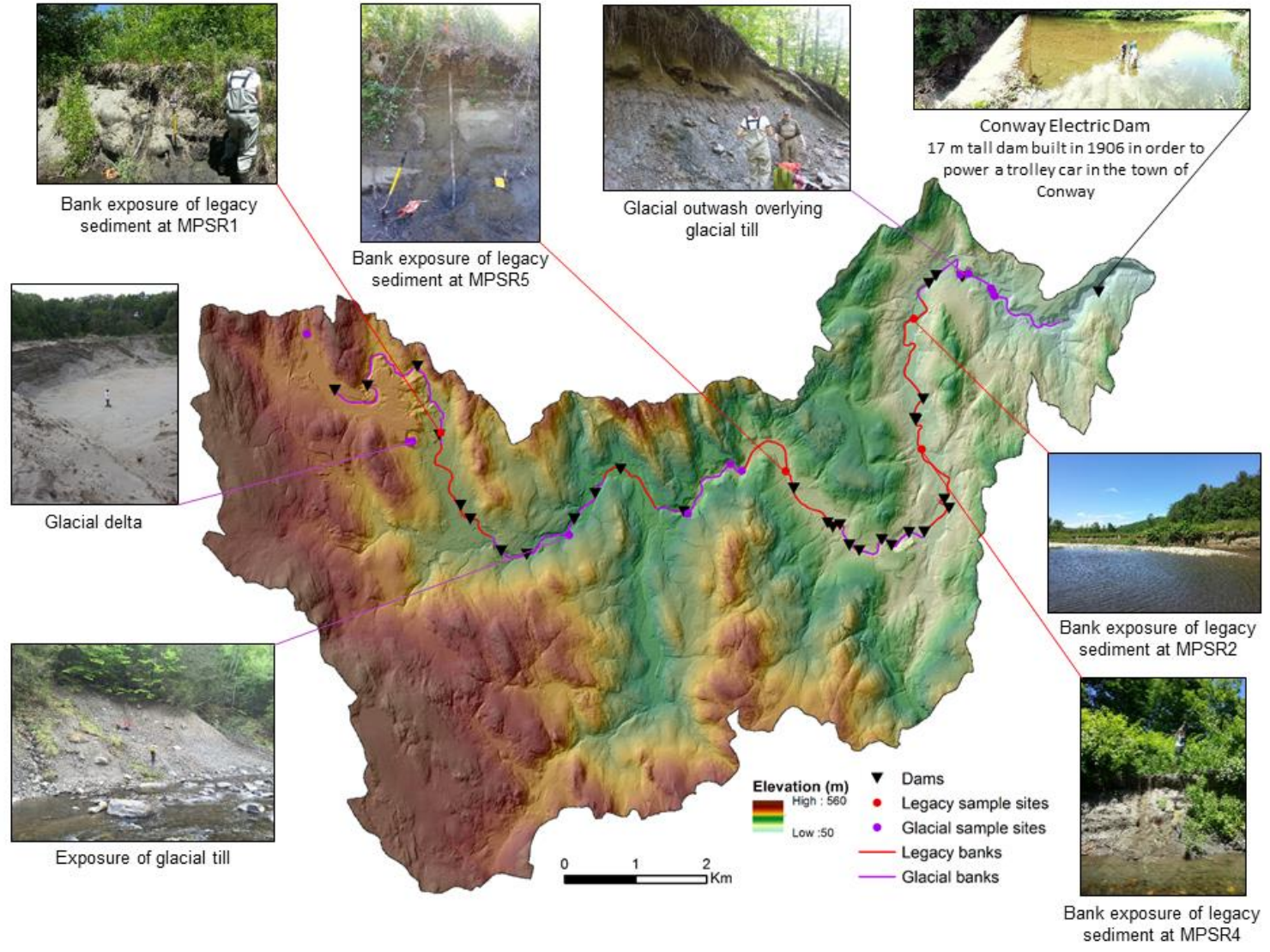
Figure 3. Map of the South River watershed showing sample locations and representative photographs of glacial and mill pond sediment exposures. Base map is 2 m LiDAR DEM.
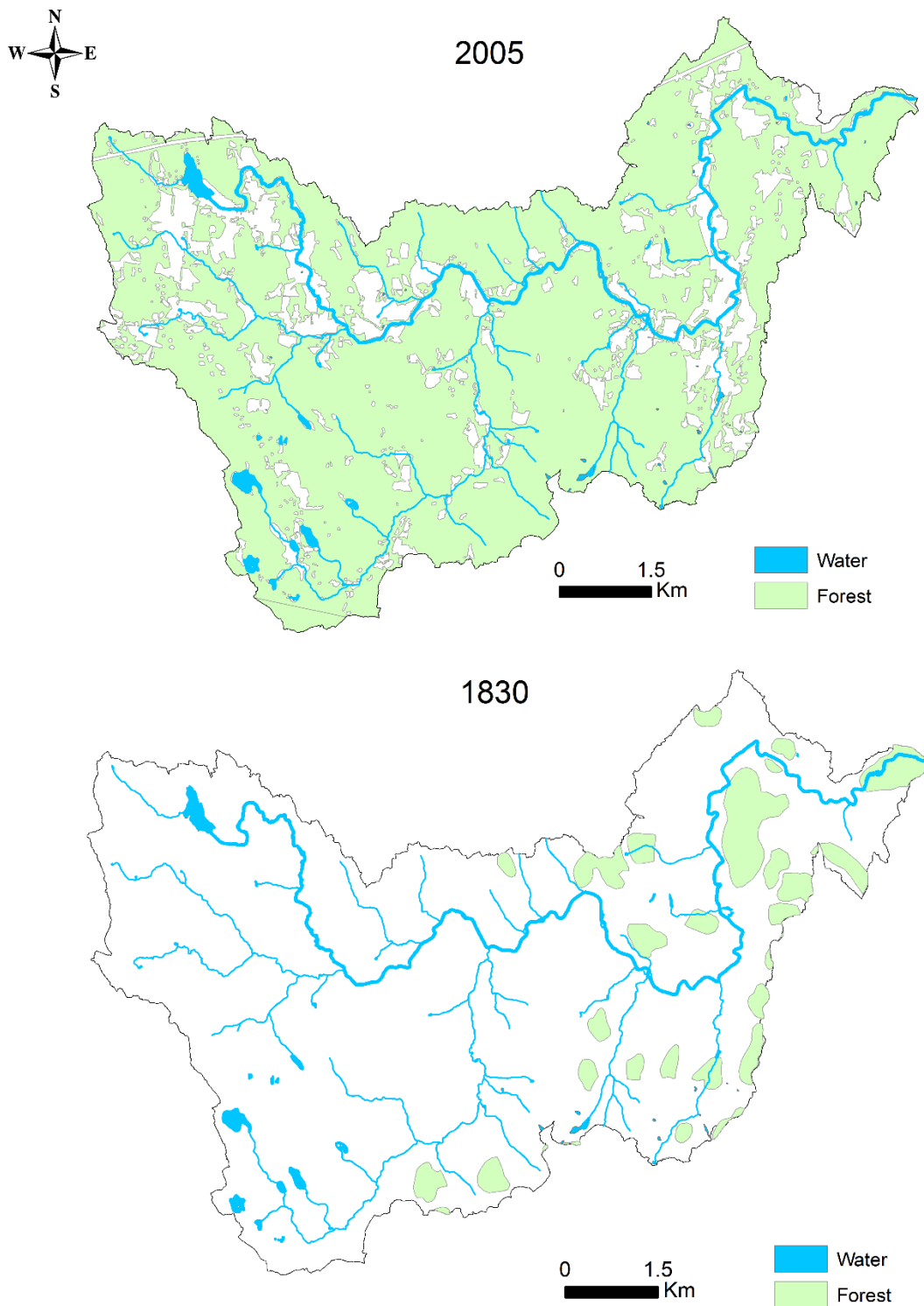
Figure 4. Forest coverage in the South River watershed for the years 2005 and 1830 (Office of Geographic Information (MassGIS), 2009; Foster and Motzkin, 2009). Green areas indicate forest cover, white indicates cleared areas for various land use activities including pasture, commercial, and residential purposes.
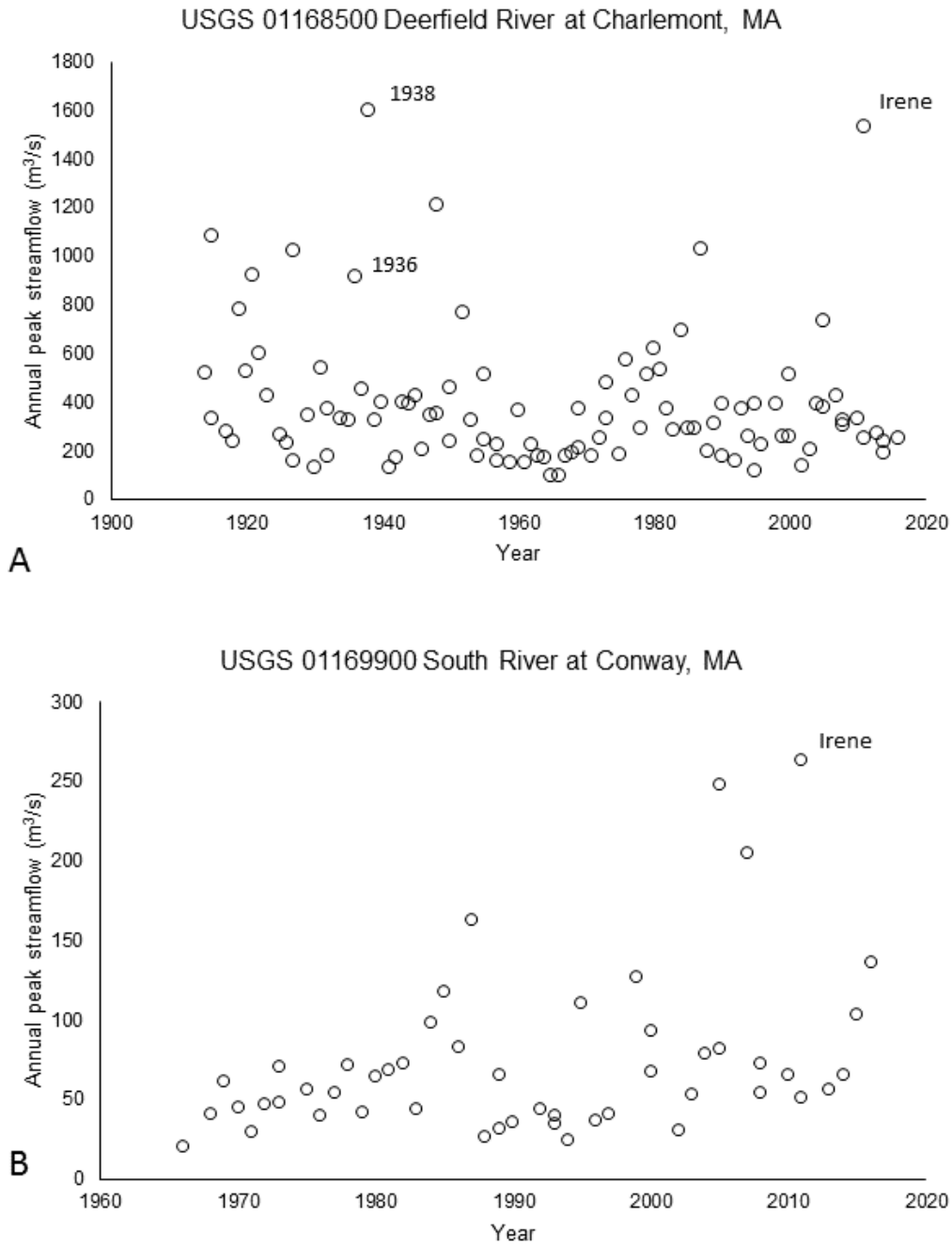
Figure 5. (A) Peak annual discharge recorded at USGS stream gage 01168500 on the Deerfield River at Charlemont, MA. Period of record begins in 1913. (B) Peak annual discharge recorded at USGS stream gage 01169900 on the South River at Conway, MA. Period of record begins in 1966. Note the recurrence interval of high events may be greater for the South River, as it is a smaller river than the Deerfield.
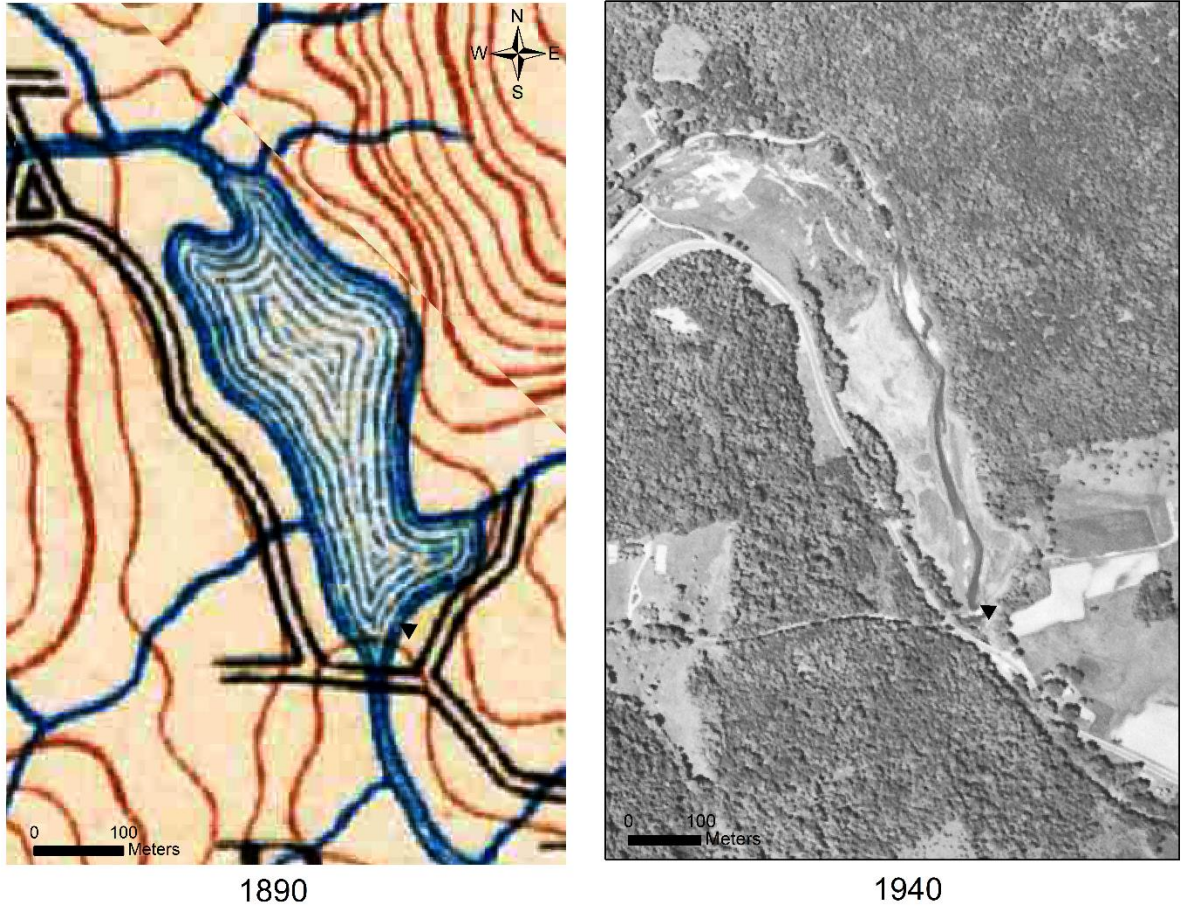
Figure 6. Location of the Conway Reservoir behind the Tucker and Cook Dam, built in 1837 (site MPSR5; Fig. 1). The left panel shows 1890 topographic map that displays evidence of a reservoir, and the right panel is a 1940 aerial photograph showing the former location of the reservoir and transition back to a river after the dam was removed in 1936. Black triangle denotes the location of the Tucker and Cook Dam.
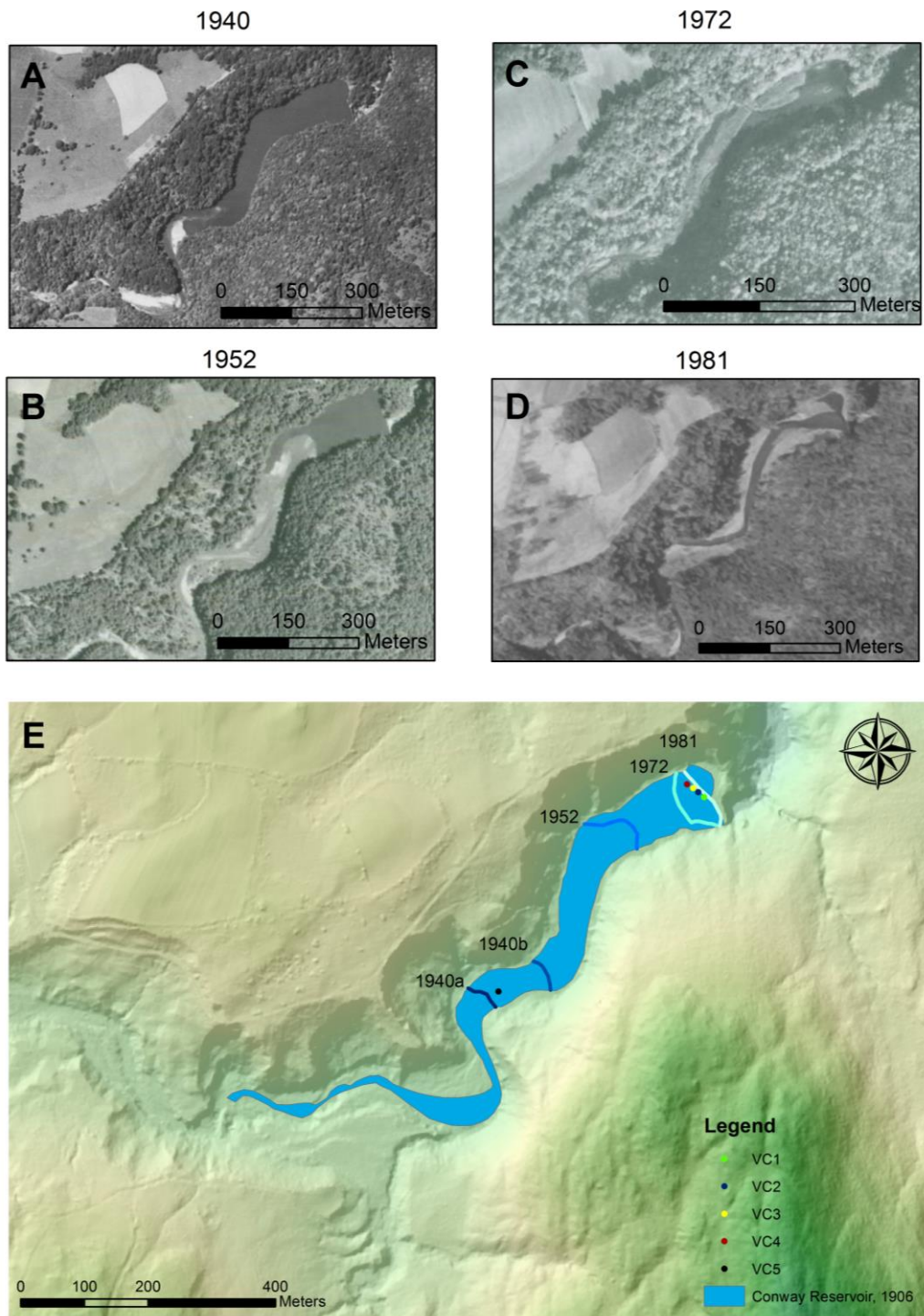
Figure 7. (A-D) Unorthorectified aerial photographs showing Conway Electric Reservoir in 1940, 1952, 1972, and 1981. (E) Map displaying the original extent of the reservoir in 1906, and the progradation of the sediment delta front for the years 1940a, 1940b (two different delta positions were interpreted and mapped from the 1940 photograph), 1952, 1972, and 1981 (from Dow, 2014). Base map is 2 m LiDAR DEM. Colored dots indicate coring locations; grainsize and geochemical analyses primarily focused on VC3 and VC5.

65
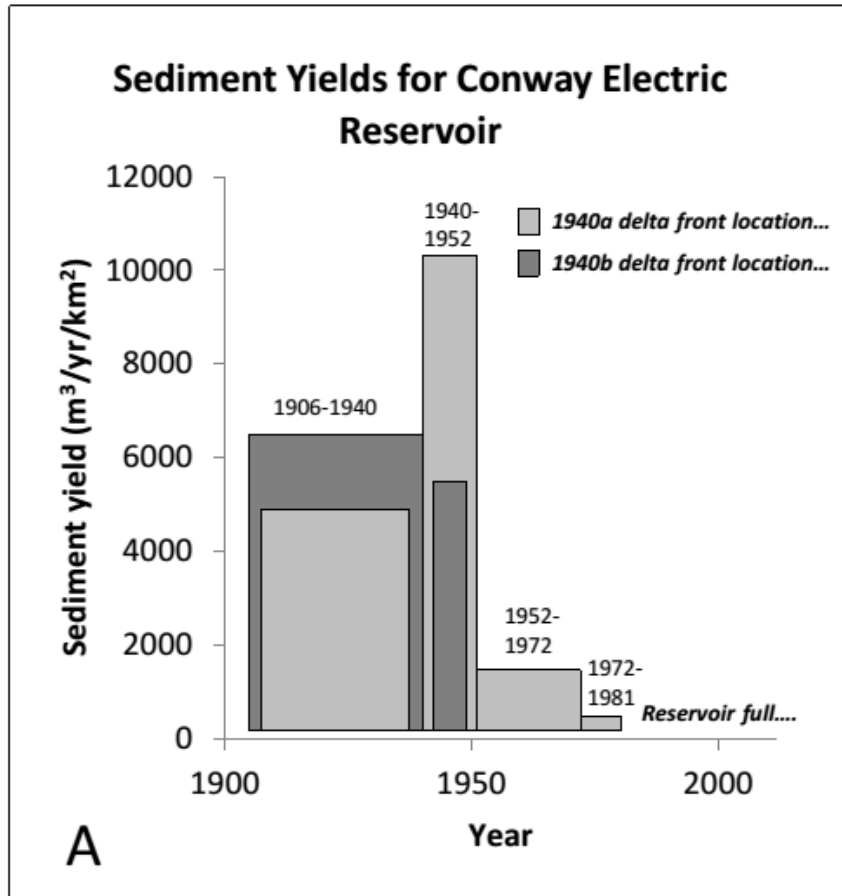
Figure 8. Sediment yield estimates calculated from sediment stored behind the Conway Electric Dam. Yield estimates for each of the time intervals correspond to delta front progradations mapped in Figure 7 (from Dow, 2014).
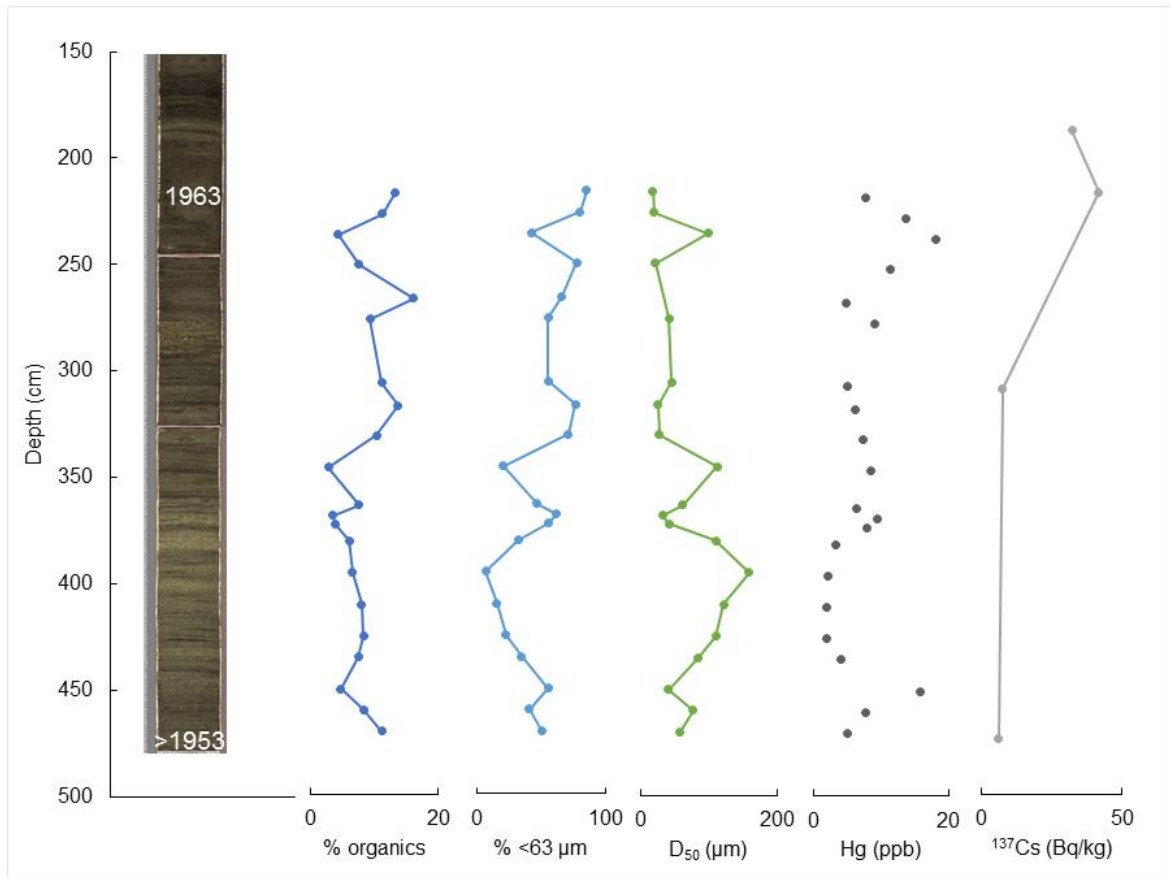
Figure 9. Median grainsize (D$_{50}$), percent organics, and concentrations of Hg, and ^{137}Cs detected in the bottom half of core VC3 at the Conway Electric Dam. The top half of the core was not sampled for geochemical analyses because material was primarily sand. Hg concentrations were normalized to organics (percent LOI). ^{137}Cs was detected at the bottom of the core, indicating a sediment age younger than 1953. The 1963 peak occurs at 213 cm. Reproduced from Dow (2014).
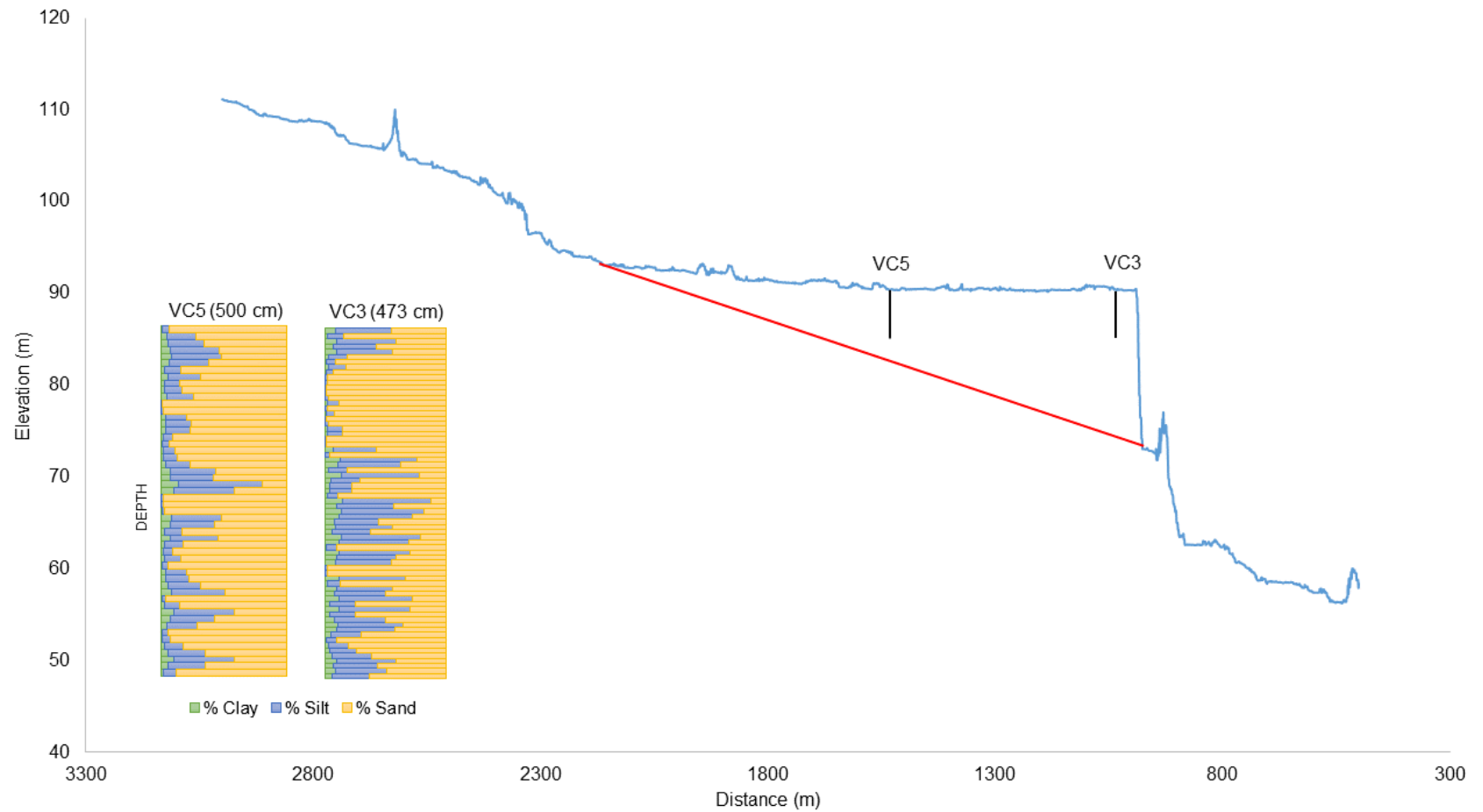
Figure 10. Longitudinal profile of the Conway Electric Dam showing locations and grainsize of cores VC3 (473 cm) and VC5 (500 cm) (Longitudinal profile is vertically exaggerated 20x). The profile was generated from LiDAR (2012, 2 m resolution). Red line is the interpreted pre-dam channel bottom.
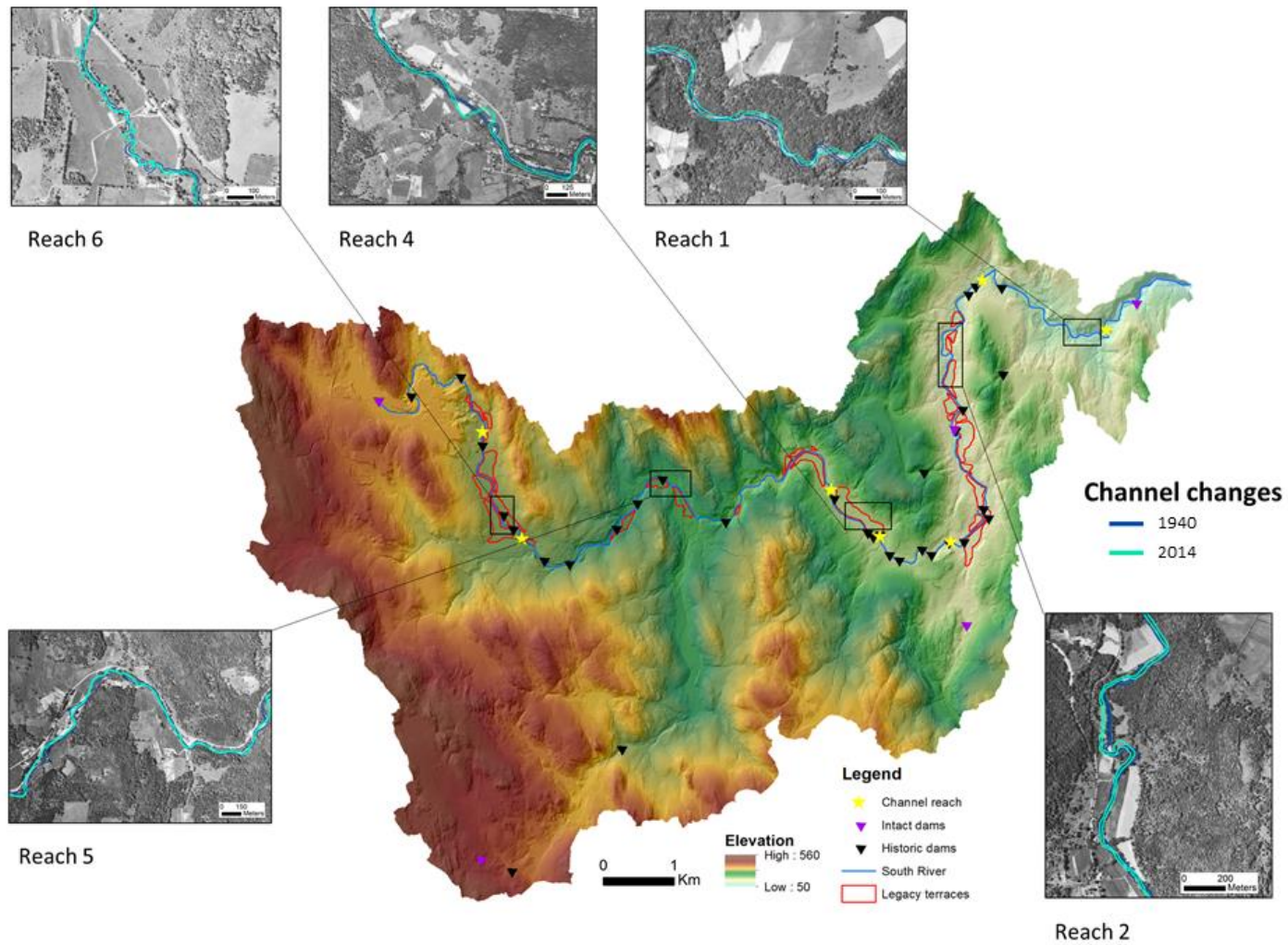
Figure 11. Map of the South River watershed showing locations of channel delineations from 1940 and 2014 for reaches of glacial and legacy sediment along the mainstem river. Reach boundaries are marked by yellow stars. Base map is 2 m LiDAR DEM. Underlying aerial photographs are from 1940.

69
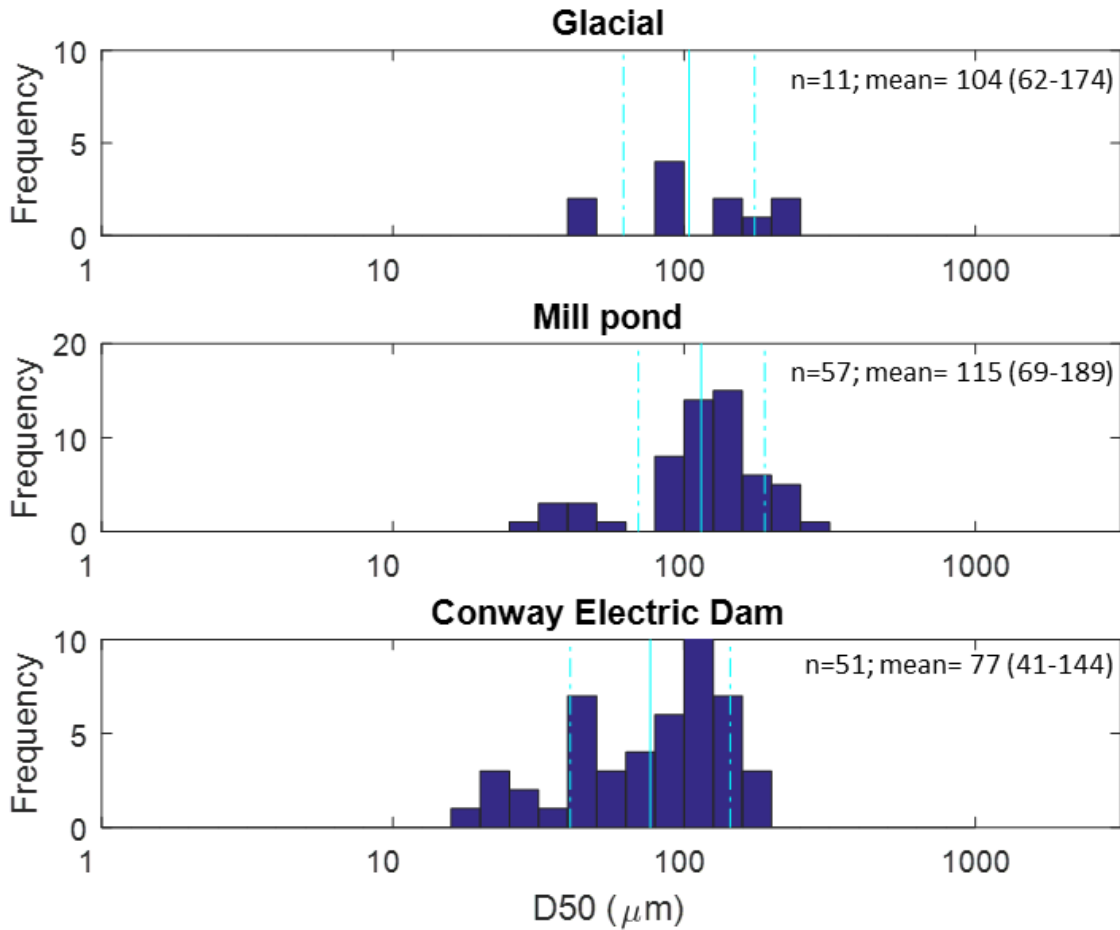
Figure 12. Histograms of median grainsize (D_{50}) for samples collected from glacial deposits, mill pond bank exposures, and at the Conway Electric Dam. Mean and range of one standard deviation reported (light blue lines), and were calculated from phi distributions that were converted back to μm.
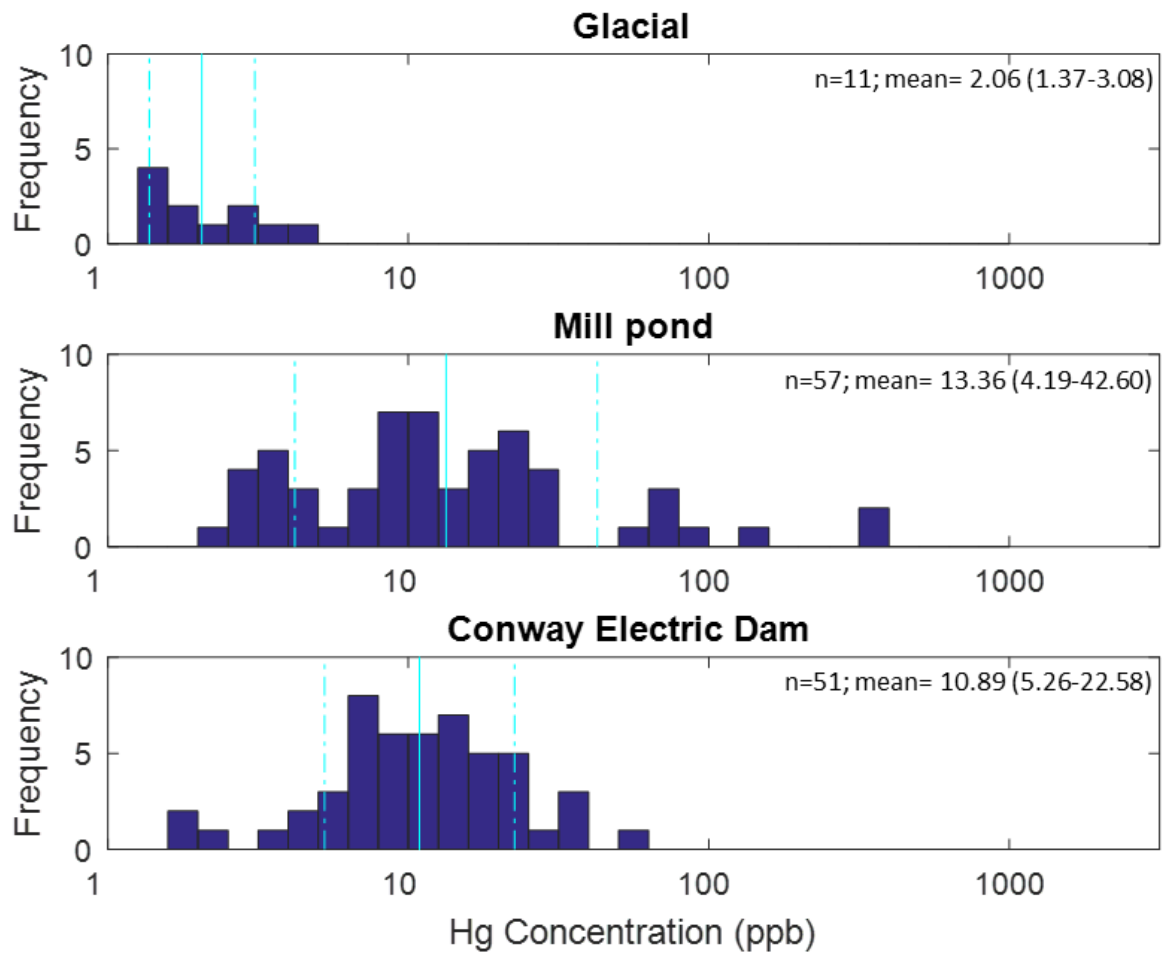
Figure 13. Histograms of mercury concentrations for samples collected from glacial deposits, mill pond bank exposures, and at the Conway Electric Dam. Concentrations are the lowest in glacial sediment, and highest in mill pond sediment. Measured Hg concentrations are normalized to organics. Mean and range of one standard deviation reported (light blue lines; Table 4), and were calculated from log transformed distributions that were converted back to ppb.
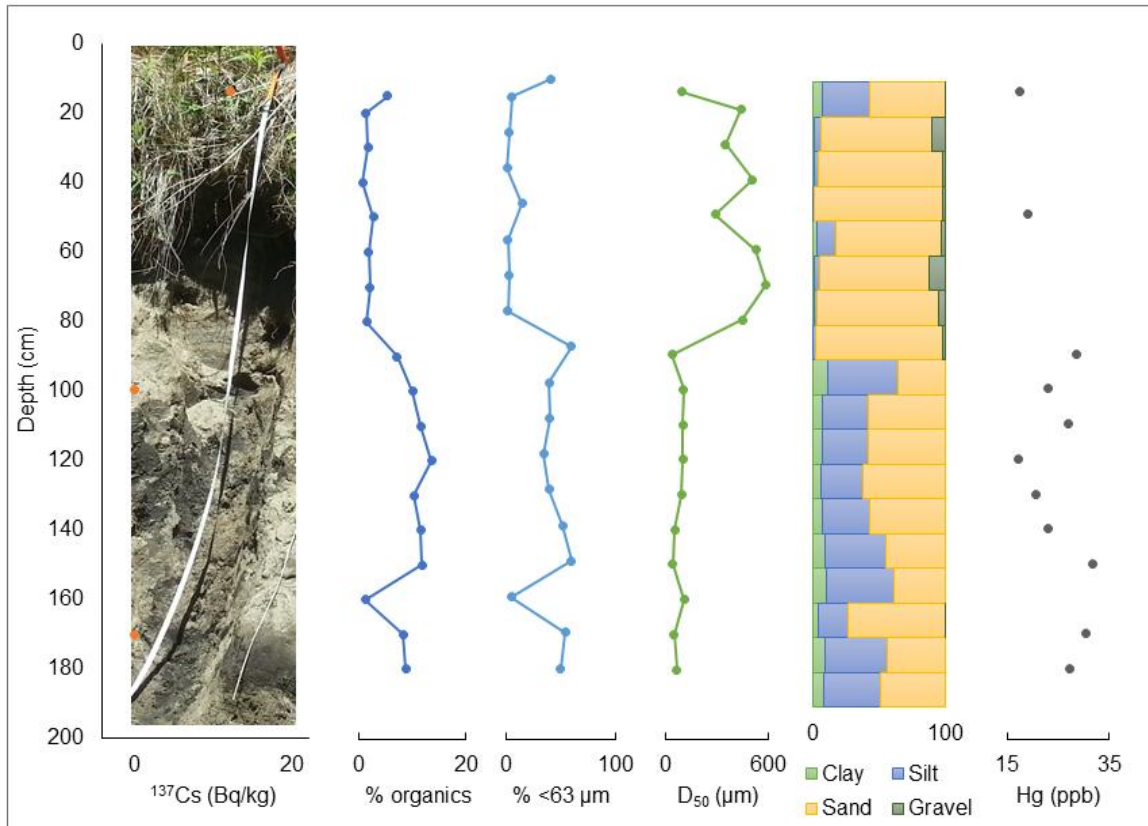
Figure 14. Profiles at legacy sediment bank exposure site MPSR1 showing ^{137}Cs, organic content (expressed as percent LOI), percent fines, grainsize (D_{50}), and Hg with depth.
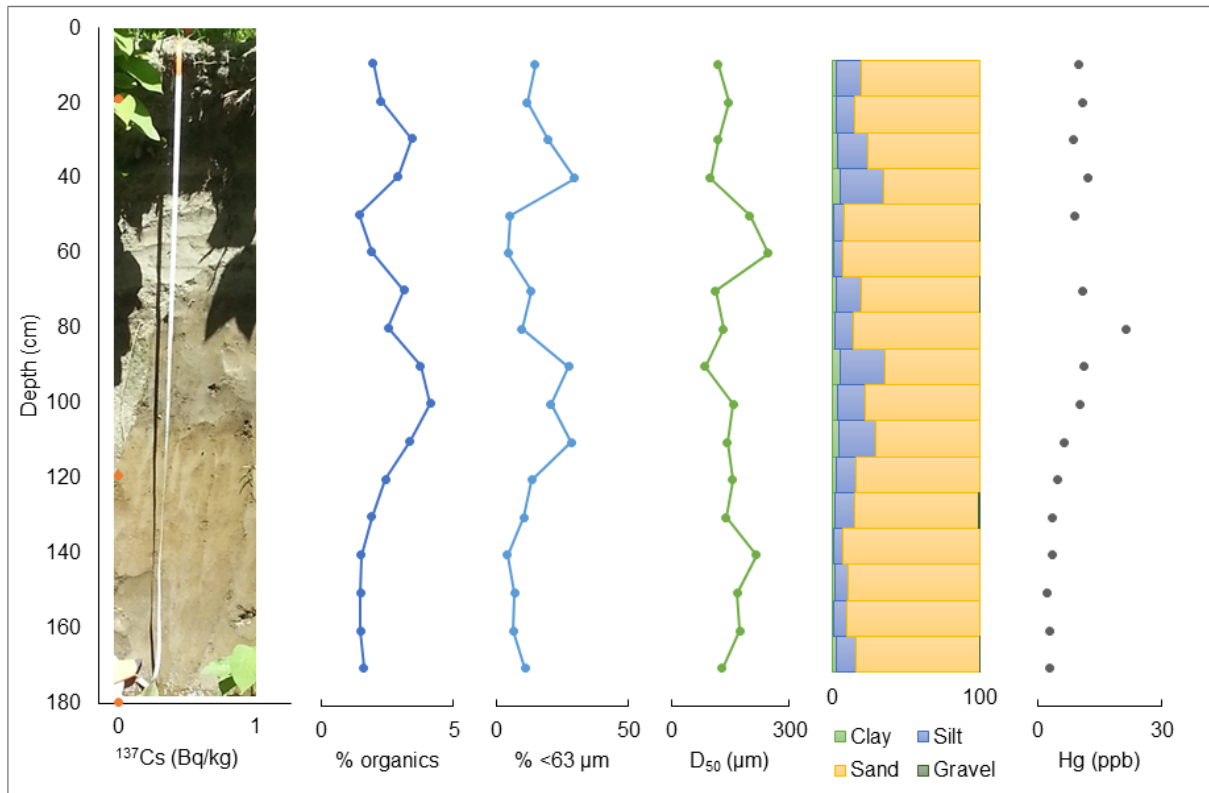
Figure 15. Profiles at legacy bank exposure site MPSR4 showing ^{137}Cs, organic content (expressed as percent LOI), percent fines, grainsize (D_{50}), and Hg with depth.
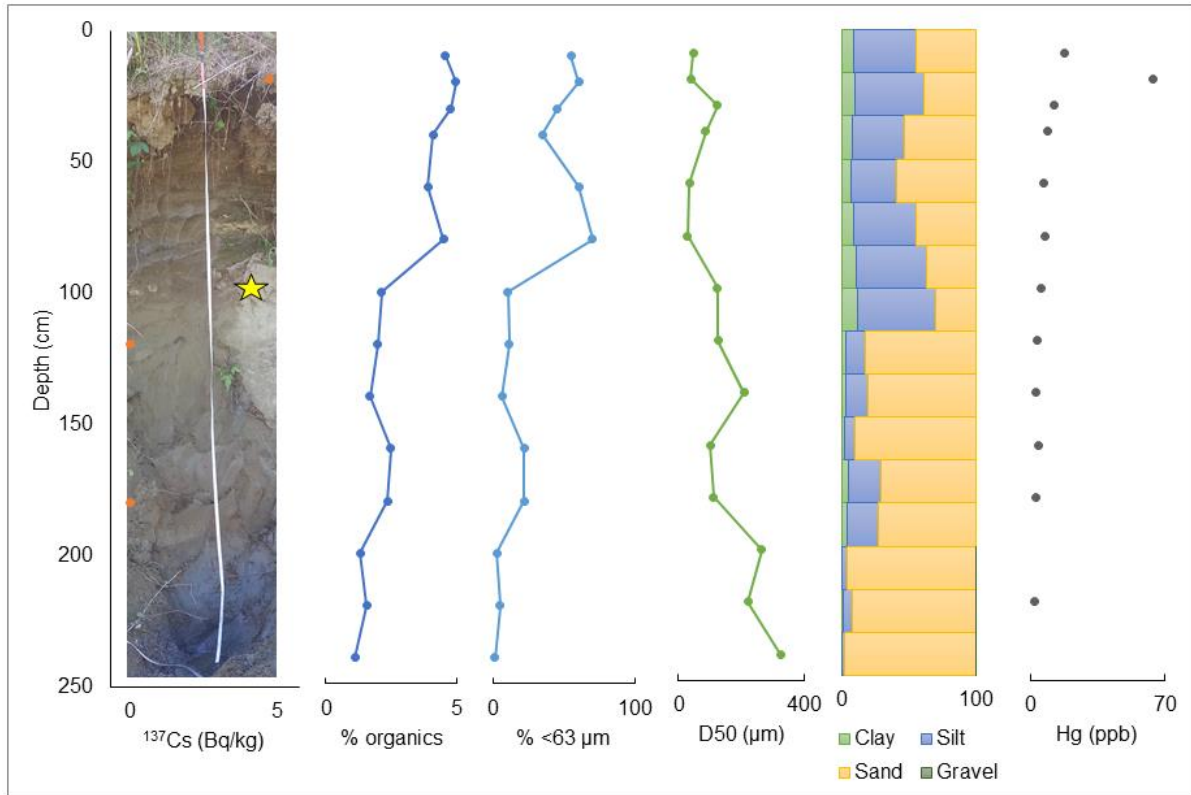
Figure 16. Profiles at legacy sediment bank exposure site MPSR5 showing ^{137}Cs, organic content (expressed as percent LOI), percent fines, grainsize (D$_{50}$), and Hg with depth. Yellow star marks a radiocarbon date with a calibrated median probable age of 1781 CE taken at 106 cm depth from the top of the bank (Johnson, 2017).
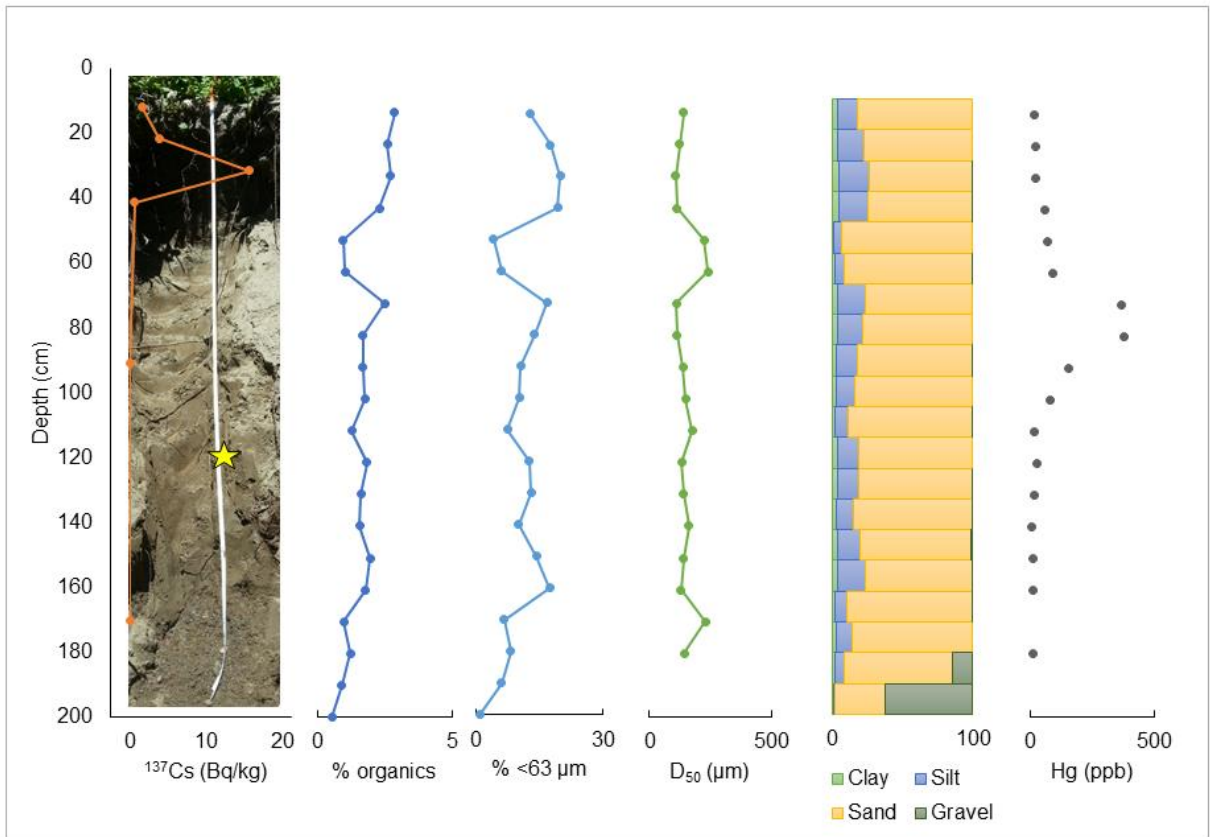
Figure 17. Profiles at legacy bank exposure site MPSR2 showing ^{137}Cs, organic content (expressed as percent LOI), percent fines, grainsize (D$_{50}$), and Hg with depth. Yellow star marks a radiocarbon date with a calibrated median probable age of 1765 CE taken at 120 cm depth from the top of the bank (Johnson, 2017).
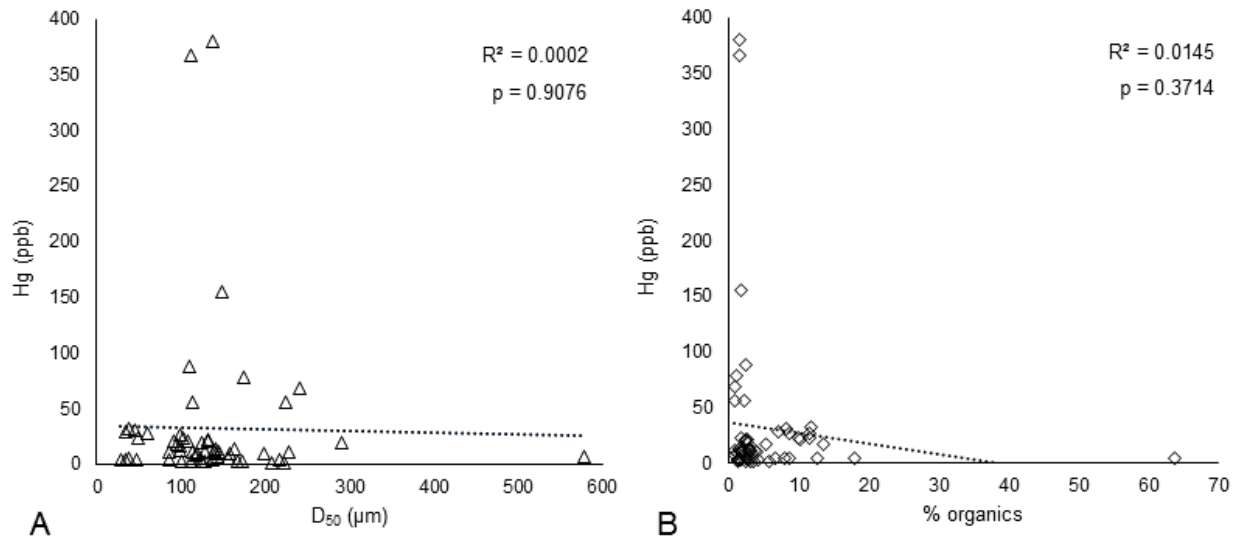
Figure 18. (A) Scatter plot showing correlation between grainsize (D$_{50}$) and Hg for legacy sediments sampled at all four sites. (B) Scatter plot showing correlation between organic content (% LOI) and Hg for legacy sediment sampled at all four sites. Hg concentrations are not correlated with both grainsize and organics.
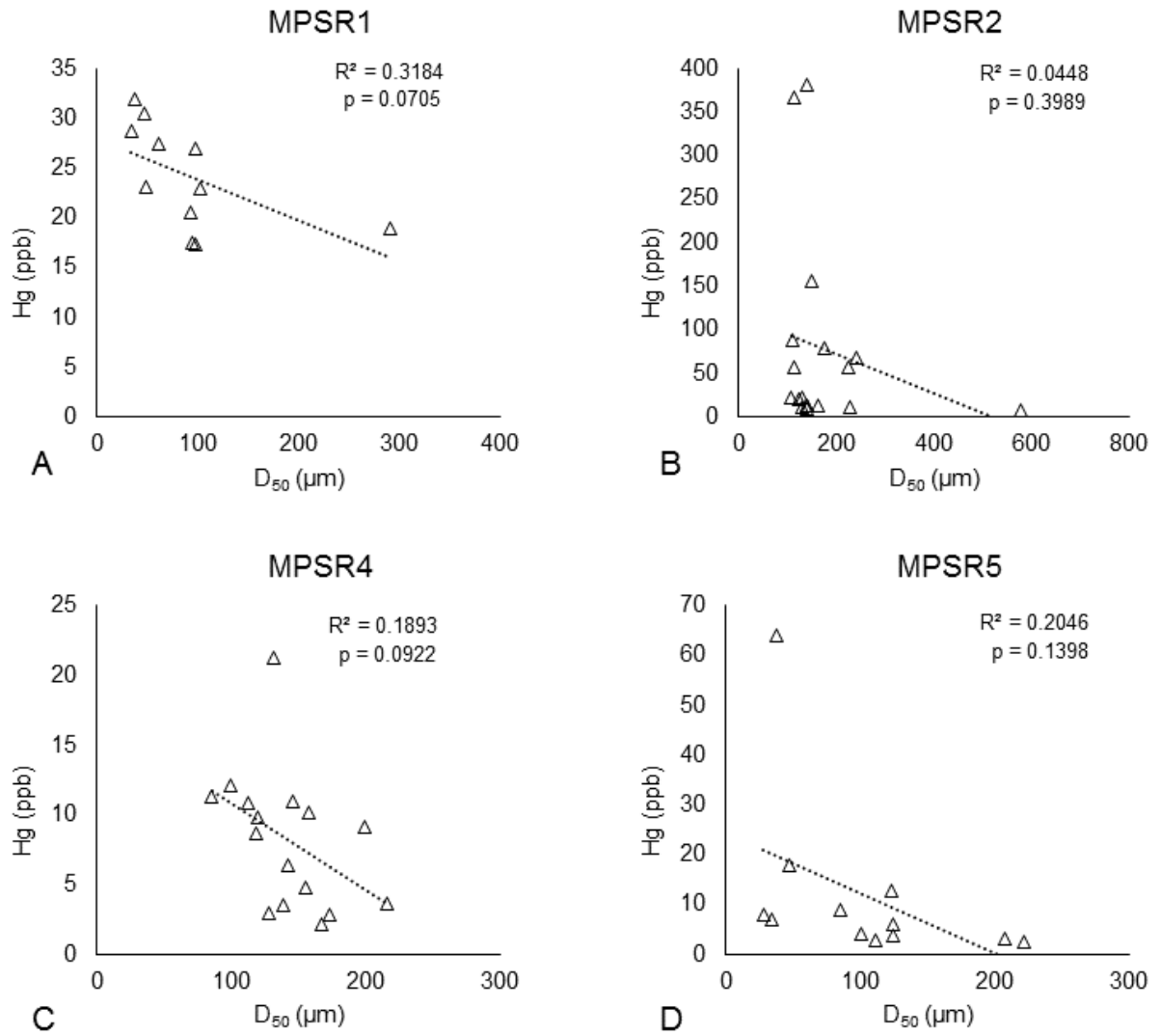
Figure 19. Scatter plot showing correlation between grainsize (D_{50}) and Hg for legacy sediments for each of the mill pond sites.
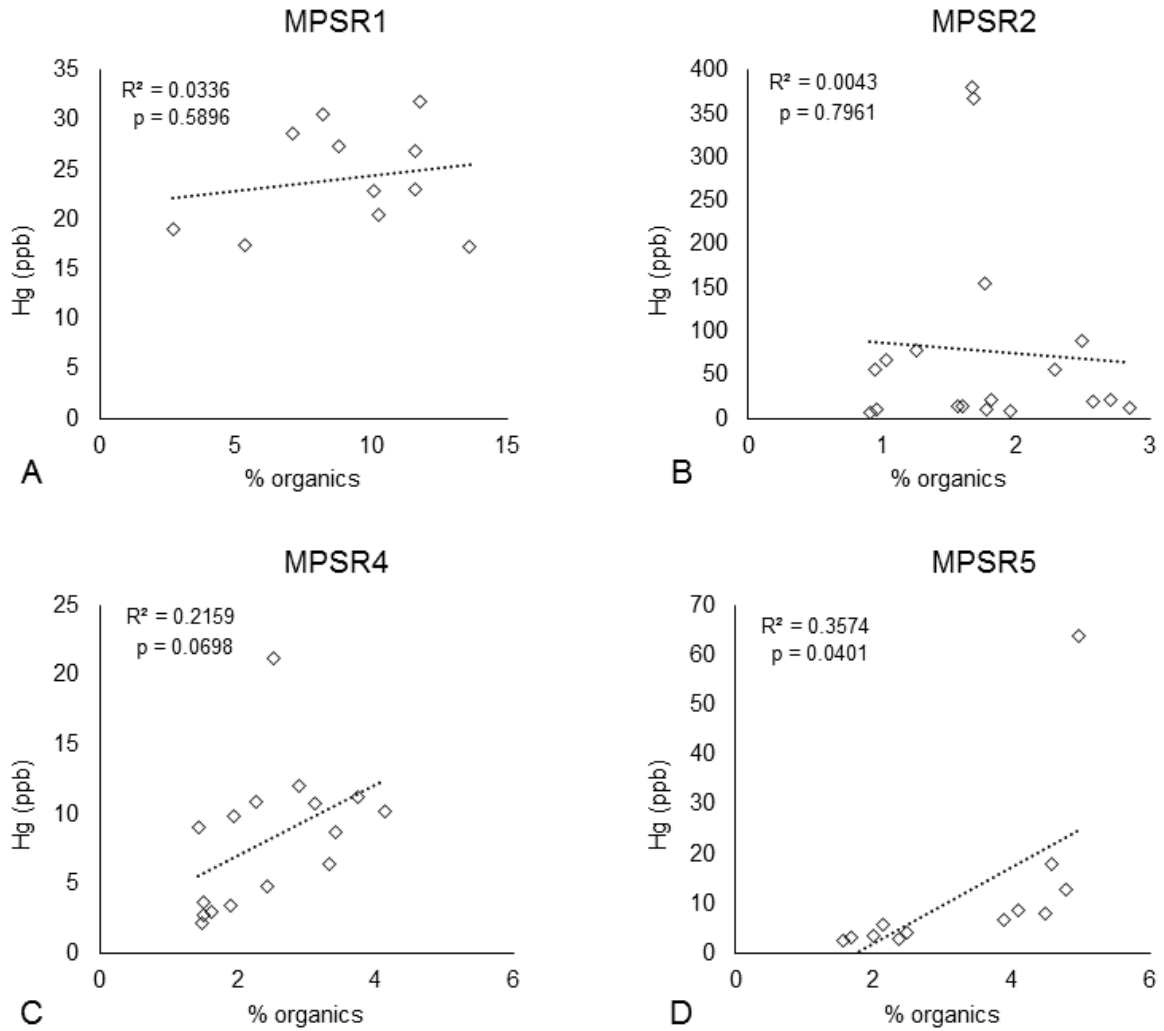
Figure 20. Scatter plot showing correlation between organics (% LOI) and Hg for legacy sediments for each of the mill pond sites.
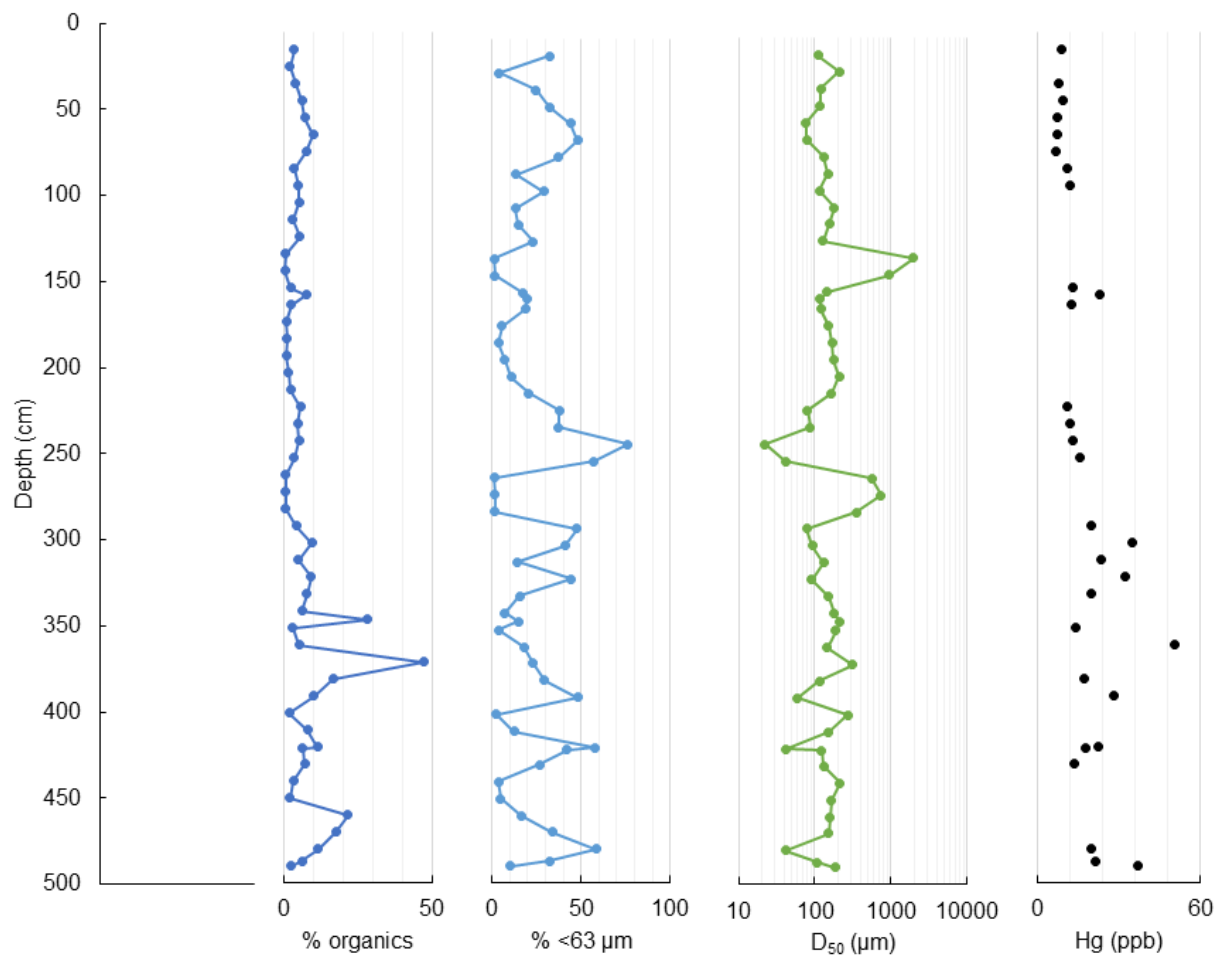
Figure 21. Median grainsize (D_{50}), percent organics, and concentrations of Hg detected in core VC5 at the Conway Electric Dam.
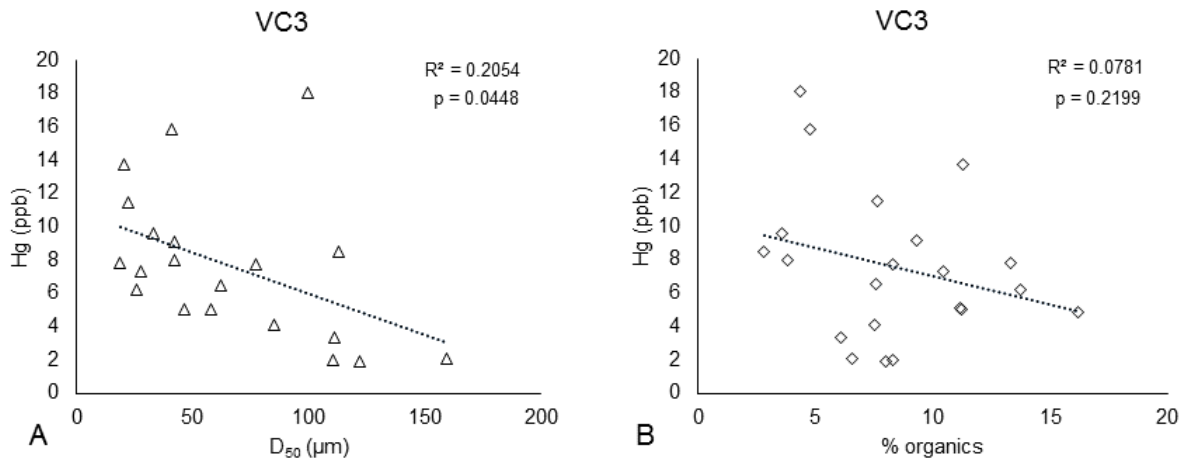
Figure 22. (A) Scatter plot showing correlation between grainsize (D_{50}) and Hg and (B) organic content and Hg for vibracore VC3 collected at the CED.
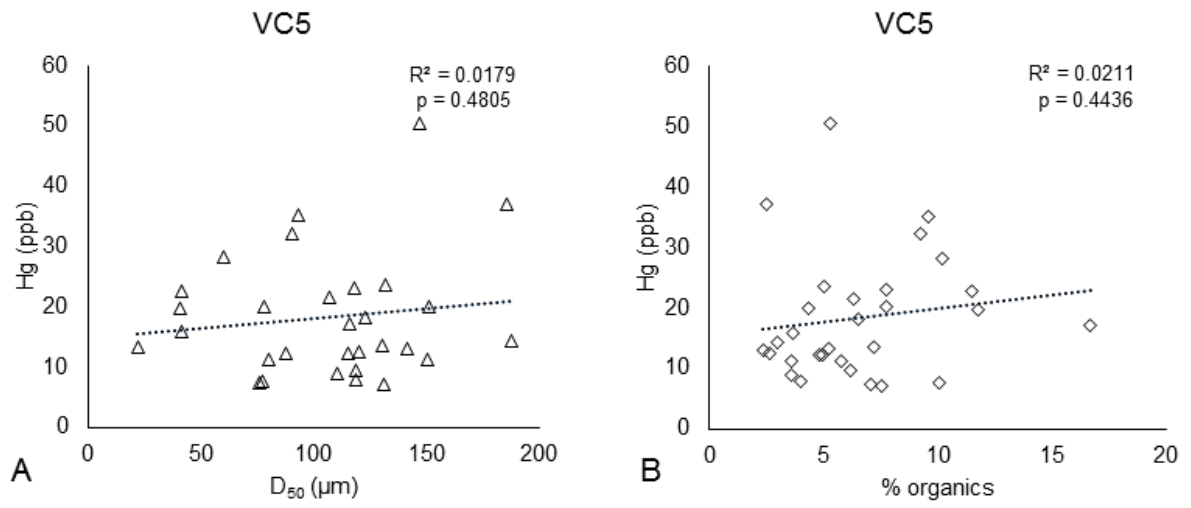
Figure 23. (A) Scatter plot showing correlation between grainsize (D_{50}) and Hg and (B) organic content and Hg for vibracore VC5 collected at the CED.
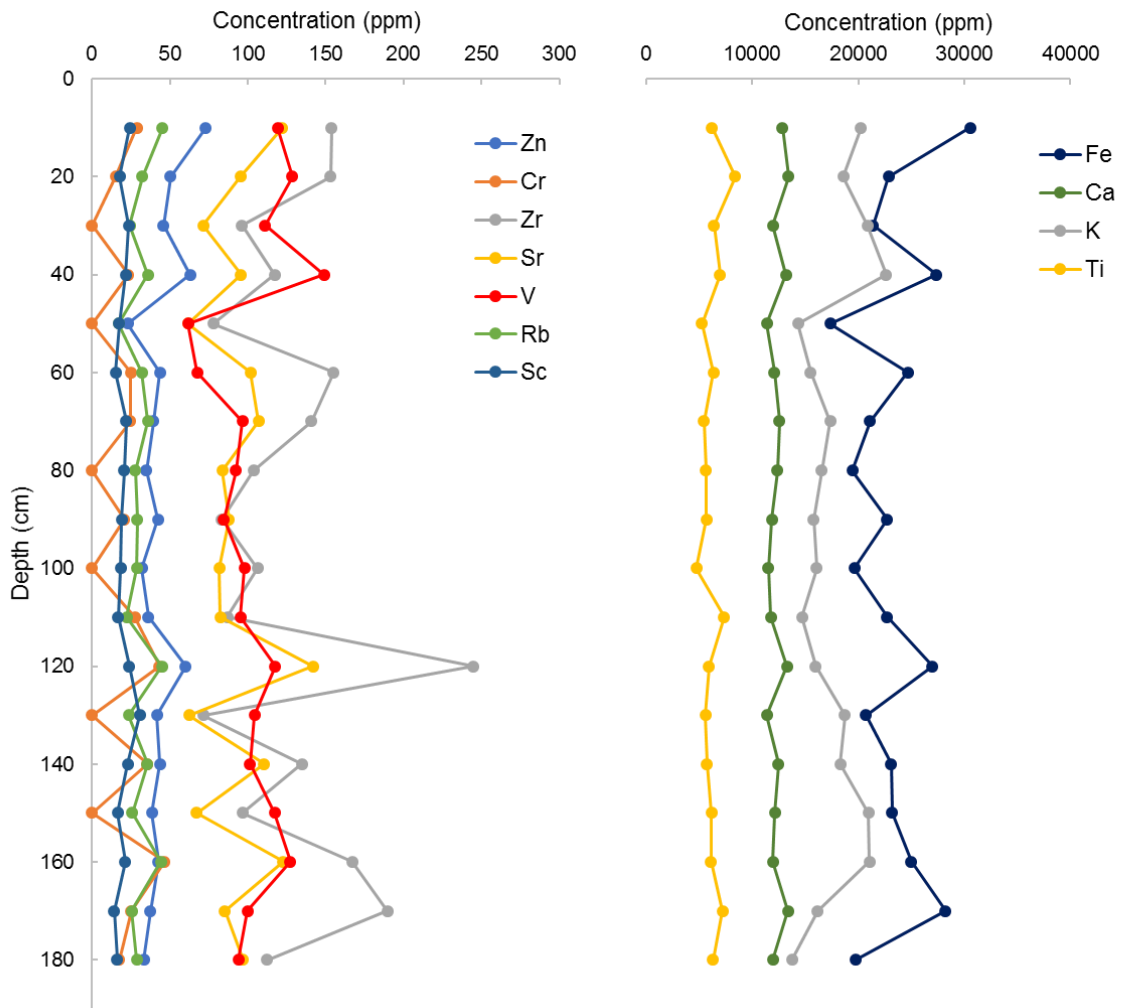
Figure 24. Elemental concentrations measured using XRF at site MPSR2. Concentrations show relatively minor variability through the bank profile. No trace metals associated with anthropogenic activity (Pb, As, Cu, Cr) were detected or were found in minor amounts using this method.
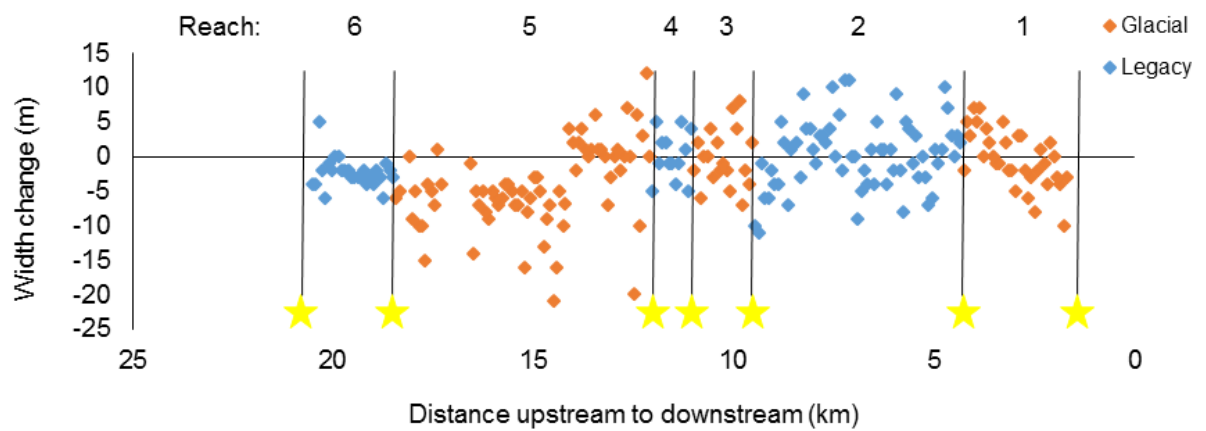
Figure 25. Change in channel width for each of the six reaches. Changes were calculated by subtracting the 1940 width from the 2014 width. Positive values indicate widening from 1940 to 2014, negative values indicate narrowing. Yellow stars indicate reach boundaries (Fig. 11).
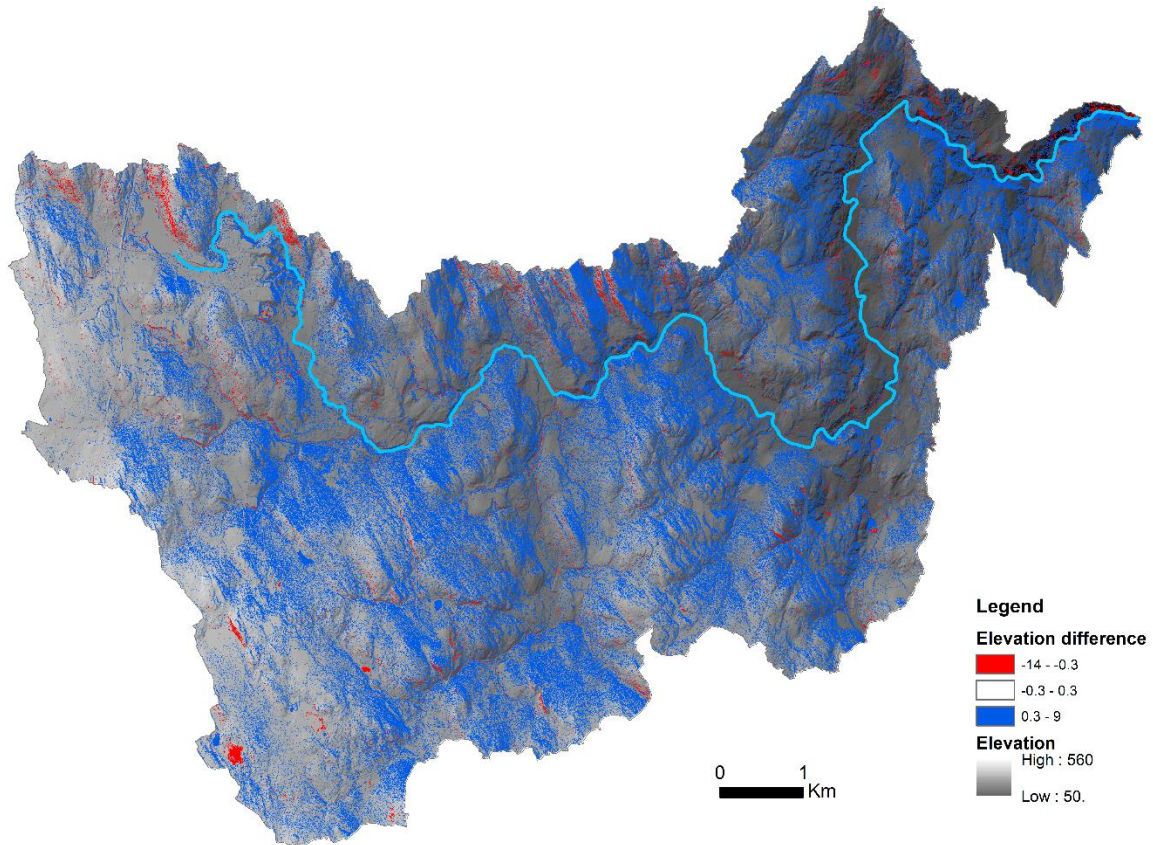
Figure 26. Areas of erosion and deposition in the South River watershed, generated by differencing LiDAR DEMs from 2015 and 2012. Base map is a hillshade generated from the 2012 LiDAR. Blue areas indicate deposition, red areas indicate erosion.